The Astrophysical Journal, 863:115 (21pp), 2018 August 20 https://doi.org/10.3847/1538-4357/aad191

On the Origin of Early Solar System Radioactivities: Problems with the Asymptotic Giant Branch and Massive Star Scenarios

D. Vescovi[1,2], M. Busso[2,3], S. Palmerini[2,3], O. Trippella[2], S. Cristallo[2,4], L. Piersanti[2,4], A. Chieffi[5,6], M. Limongi[7,8], P. Hoppe[9], and K.-L. Kratz[10]

[1] Gran Sasso Science Institute, Viale Francesco Crispi, 7, I-67100 L'Aquila, Italy; diego.vescovi@gssi.it
[2] INFN, Section of Perugia, Via A. Pascoli snc, I-06123 Perugia, Italy
[3] University of Perugia, Department of Physics and Geology, Via A. Pascoli snc, I-06123 Perugia, Italy
[4] INAF, Observatory of Abruzzo, Via Mentore Maggini snc, I-64100 Collurania, Teramo, Italy
[5] INAF—Istituto di Astrofisica e Planetologia Spaziali, Via Fosso del Cavaliere 100, I-00133, Roma, Italy
[6] Monash Centre for Astrophysics, School of Mathematical Sciences, Monash University, Victoria 3800, Australia
[7] INAF—Osservatorio Astronomico di Roma, Via Frascati 33, I-00040, Monteporzio Catone, Italy
[8] Kavli Institute for the Physics and Mathematics of the Universe, Todai Institutes for Advanced Study, University of Tokyo, Kashiwa, 277-8583 (Kavli IPMU, WPI), Japan
[9] Max-Planck-Institut für Chemie, Hahn-Meitner-Weg 1, D-55128 Mainz, Germany
[10] Fachbereich Chemie, Pharmazie & Geowissenschaften, Mainz Universität, Fritz-Strassmann-Weg 2, D-55128 Mainz, Germany
Received 2018 February 10; revised 2018 June 6; accepted 2018 July 2; published 2018 August 16

Abstract

Recent improvements in stellar models for intermediate-mass stars and massive stars (MSs) are recalled, together with their expectations for the synthesis of radioactive nuclei of lifetimes $\tau \lesssim 25$ Myr, in order to re-examine the origins of now extinct radioactivities that were alive in the solar nebula. The Galactic inheritance broadly explains most of them, especially if *r*-process nuclei are produced by neutron star merging, according to recent models. Instead, ^{26}Al, ^{41}Ca, ^{135}Cs, and possibly ^{60}Fe require nucleosynthetic events close to the solar formation. We outline the persisting difficulties to account for these nuclei by intermediate-mass stars ($2 \lesssim M/M_{\odot} \lesssim 7$–8). Models of their final stages now predict the ubiquitous formation of a ^{13}C reservoir as a neutron capture source; hence, even in the presence of ^{26}Al production from deep mixing or hot bottom burning, the ratio ^{26}Al/^{107}Pd remains incompatible with measured data, with a large excess in ^{107}Pd. This is shown for two recent approaches to deep mixing. Even a late contamination by an MS encounters problems. In fact, the inhomogeneous addition of supernova debris predicts nonmeasured excesses on stable isotopes. Revisions invoking specific low-mass supernovae and/or the sequential contamination of the presolar molecular cloud might be affected by similar problems, although our conclusions here are weakened by our schematic approach to the addition of SN ejecta. The limited parameter space that remains to be explored for solving this puzzle is discussed.

Key words: nuclear reactions, nucleosynthesis, abundances – Sun: evolution – stars: AGB and post-AGB – stars: evolution – stars: massive

1. Short-lived Radioactivities in the Early Solar System (ESS)

Measurements revealing that several radioactive species with half-lives ranging from less than one to hundreds of million years were present in solids in the ESS have gradually accumulated in the past decades, after the pioneering work by Reynolds (1960) on ^{129}I. These nuclei are, in the present context, referred to as *short-lived radioactivities* (SLRs).

Identification today of the stable decay product (and of its abundance) for a nucleus of this kind permits one to extrapolate backward, deriving the original abundance of the unstable isotope (Busso et al. 1999; Wasserburg et al. 2006; Davis & McKeegan 2014). A description of the procedure can be found, e.g., in Lee et al. (1976). Figure 1 shows this technique, as applied to ^{26}Al and ^{41}Ca; the figure is taken from the work by Sahijpal et al. (1998).

There is now a tremendous wealth of new measurements on ESS samples. It then poses the crucial question of the astrophysical interpretation of their presence: this problem is still partly unsolved now. It is in any case evident that although solid materials formed in a very short lapse of time (from a fraction of a megayear to a few megayears), they somehow maintain a record of several phenomena, from the possible blend of various stellar nucleosynthetic processes (Busso 2011, 2018) to traces of spallation effects induced in the solar nebula itself (Sossi et al. 2017). For a detailed account of the science built in the last 60 years with short-lived nuclei we refer the reader to dedicated reviews—see, e.g., Busso et al. (1999), Kratz et al. (2004), Wasserburg et al. (2006), Wadhwa et al. (2007), Huss et al. (2007), Davies et al. (2014), and Davis & McKeegan (2014).

Some of the experimental estimates for early SLR abundances are still uncertain and subject to discussion. This is often true for nuclei of metals that are extremely difficult or impossible to measure in pristine refractory condensates, so that their inferred initial abundances in the ESS require extrapolations from measurements made on subsequent, differentiated objects. In this field the case of ^{60}Fe is of particular importance. The values derived for the initial abundance ratio ^{60}Fe/^{56}Fe span a wide range of a few 10^{-9} (Tang & Dauphas 2012) to about 10^{-6} (Mostefaoui et al. 2005). A review by Davis & McKeegan (2014) discusses in some detail how the inference of an initial ratio based on absolute age determinations for eucrite samples where it was measured early on is bound to suffer from large systematic uncertainties. Those authors privileged the lowest values presented in the literature; however, there does not seem to exist a general agreement on this, especially in view of the

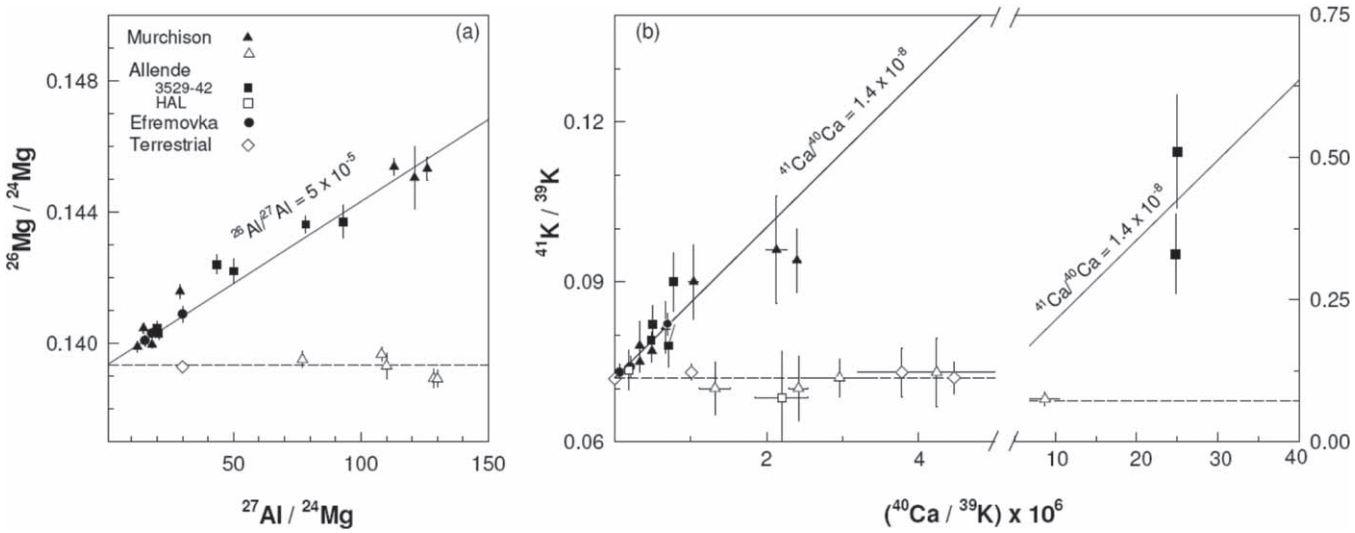

Figure 1. Panel (a) shows the Al–Mg data from calcium and aluminum inclusions (CAIs) in various meteorites; the straight-line fit to the filled symbols is for the so-called canonical value of $(^{26}Al/^{27}Al)_0$ in the ESS, $\simeq 5 \cdot 10^{-5}$. Panel (b) shows the Ca–K data from the same samples used for Panel (a). The first measurements and the line pointing to $(^{41}Ca/^{40}Ca)_0 = 1.4 \cdot 10^{-8}$ are derived from Srinivasan et al. (1994, 1996). The suggestion of a correlation with Al is based on Sahijpal et al. (1998). This figure is reproduced from the latter study and from Wasserburg et al. (2006). Copyright: Nature Publishing Group. (Note that a subsequent work by Liu et al. (2012) has proved that the initial ^{41}Ca abundance was lower at the level of $(^{41}Ca/^{40}Ca)_0 \backsim 4.2 \cdot 10^{-9}$.)

possible large internal modifications of the abundances in the samples, subsequent to the solar system's formation (Telus et al. 2016; see also Boss 2017). The most recent measurements by Trappitsch et al. (2018) stay in the lower part of the spread but suggest an initial abundance considerably higher than the choice of Davis & McKeegan (2014). We shall therefore consider this isotopic ratio to be uncertain inside the wide range of 10^{-8} to 10^{-6}.

In Table 1 we try to fix reasonable ESS abundance ratios $([N^R/N^S]_{Meas.})$ for SLRs with a mean life (τ_R) shorter than 25 Myr. We also include ^{146}Sm as an example of longer-lived nuclei. We adopt mainly Davis & McKeegan (2014) as a reference; this will be generally adequate for our purposes, with the mentioned exception of ^{60}Fe.

In the last 40 years a wealth of astrophysical models have been presented in an attempt to account for the presence of short-lived nuclei in early solar materials. The first interpretation was advanced by Cameron & Truran (1977), who suggested that a supernova (SN) that occurred close in time and space to the solar nebula formation might have introduced the required nucleosynthetic contaminations. After that seminal work, the idea of a close encounter with a dying star was re-explored by many authors, and various stellar scenarios were examined, from that of a single SN to that of a less massive object—namely, a low- or intermediate-mass star in its asymptotic giant branch (AGB) phase (Podosek & Nichols 1997; Wasserburg et al. 1998, 2006; Busso et al. 1999; Gounelle et al. 2006; Takigawa et al. 2008; Huss et al. 2009).

The evolution of ejecta from massive stars (MSs) has also been modeled by various authors. These works range from studies of cosmic ray processes inside SN remnants, where even ^{10}Be can be produced (Tatischeff et al. 2014), to the reconstruction of the evolution of a molecular cloud possibly hosting the solar nebula, with its complex phenomena of nucleosynthesis from previous SNe, mixing, and contributions from very massive stars in their Wolf–Rayet (WR) stage (see, e.g., Gounelle & Meynet 2012; Dwarkadas et al. 2017, 2018; and references therein).

Table 1
Short-lived Nuclei in the ESS[a]

Rad.	Ref.	τ_R (Myr)	$[N^R/N^S]_{Meas.}$
^{10}Be	^{9}Be	2.0	$(8.8 \pm 0.6) \cdot 10^{-4}$
^{26}Al	^{27}Al	1.03	$(5.23 \pm 0.13) \cdot 10^{-5}$
^{36}Cl	^{35}Cl	0.43	$1.8 \cdot 10^{-5}$
^{41}Ca	^{40}Ca	0.15	$4 \cdot 10^{-9}$
^{53}Mn	^{55}Mn	5.3	$(6.7 \pm 0.56) \cdot 10^{-6}$
^{60}Fe	^{56}Fe	3.75	10^{-8}–10^{-6}
^{107}Pd	^{108}Pd	9.4	$(5.9 \pm 2.2) \cdot 10^{-5}$
^{129}I	^{127}I	23	$1.0 \cdot 10^{-4}$
^{135}Cs	^{133}Cs	3.3	$4.8 \cdot 10^{-4}$
^{182}Hf	^{180}Hf	12.8	$(9.81 \pm 0.41) \cdot 10^{-5}$
^{205}Pb	^{204}Pb	22	10^{-3}
^{247}Cm	^{232}Th	23	$(1.1–2.4) \cdot 10^{-3}$
^{146}Sm	^{144}Sm	148	$1.0 \cdot 10^{-2}$

Note.
[a] For general references see Wasserburg et al. (2006) and Davis & McKeegan (2014). For recently revised abundances see Chaussidon et al. (2006) for ^{10}Be, Tang & Dauphas (2012) for ^{60}Fe, Schönbächler et al. (2008) for ^{107}Pd, Hidaka & Yoneda (2013) for ^{135}Cs, Burkhardt et al. (2008) for ^{182}Hf, Baker et al. (2010) for ^{205}Pb, and Brennecka et al. (2010) for ^{247}Cm.

Various objections have been raised to each of the models presented (for an inventory of these see, e.g., Busso 2011, 2018). Basically, the most relevant ones can be divided into two categories, each involving a different mass range of the proposed source. First of all, any idea involving an SN event or a sequence of SN contributions in a molecular cloud must keep in mind that these explosive phenomena are the main source of nucleosynthesis for most of the stable elements—for α-rich ones in particular. As suggested by Wasserburg et al. (1998), materials derived from SN nucleosynthesis and diluted sufficiently to account for the ^{26}Al and ^{60}Fe concentrations in the ESS are bound to contain large amounts of oxygen, neon, magnesium, silicon, etc. Their inclusion would affect the early solar nebula in completely different ways, depending on how

they are added to the materials of the forming star. Let us consider in more detail this crucial point. A first possibility is that fresh core collapse SN (CCSN) ejecta are directly added to the forming solar system by a single event (maybe also triggering the collapse), maintaining the typical, heterogeneous structure characterizing SN remnants (Loll et al. 2013; Boss 2017). This nonhomogeneous and clumpy kind of mixing was first modeled by Pan et al. (2012); in this case, the effects of the pollution should be now registered in pristine meteorites in the form of widespread anomalies in the abundance ratios of stable isotopes for such elements, at the level of a few percent (Wasserburg et al. 1998). The most important of these effects would concern oxygen, generally produced in large quantities by exploding stars leaving a neutron star as a remnant. However, observed oxygen isotope anomalies in primitive solar system materials do not require the admixture of a distinct nucleosynthetic component (see Section 2). Anomalies in contrast with observations would also be predicted for the isotopes of other α-rich nuclei, and significant excess would be foreseen for SLR ^{53}Mn, whose ratio to ^{55}Mn would be higher than observed by orders of magnitude (Wasserburg et al. 1998; Meyer & Clayton 2000); the whole scenario is therefore in doubt. Attempts at answering these objections have invoked very peculiar SN types, e.g., objects ejecting only external layers, not influenced by manganese production (Meyer & Clayton 2000), and those having a particular mass (close to the lowest limit for CCSNe), to minimize the production of unwanted anomalies in oxygen- and α-rich nuclei (Banerjee et al. 2016). In any case, whatever ad hoc choice of parameters is adopted, these models do not really avoid the problems outlined above. An example is the recent work by Banerjee et al. (2016), where abundance shifts not acceptable by the present meteoritic measurements (i.e., at levels of 1%–3%) remain on various stable isotopes (see Table 3 in their supplemental materials).

A very different scenario considers that before being admixed into the presolar nebula, the ejecta of previous SNe had time to mix and homogenize in the molecular cloud from which the Sun formed, presumably because they came from an appreciable number of explosive events in a sequential star formation process lasting for several million years. If this was the case for the solar formation, the addition of the most stable nuclei would not cause any particular problem: they would simply modify slightly the "average" solar abundances, not introducing measurable isotopic variations with respect to the average composition in pristine meteorites. This type of scenario has been rather common in recent years (Gounelle & Meynet 2012; Dwarkadas et al. 2017). On the one hand, this scheme might appear rather realistic and is indeed interesting in itself, offering an alternative to single-star contamination. Some versions of it indicate that a late-WR star may have provided adequate amounts of ^{26}Al (and maybe ^{60}Fe) from stellar winds. The presence of other SLRs with different lifetimes would be simply the fossilized record of sequential star formation within a hierarchical interstellar medium (ISM). However, as we shall see, a major problem in this case emerges for the excess of unstable ^{53}Mn. While for a single event one might accept that the contaminant was a rare, peculiar SN, where Mn was not ejected, at the level of a whole molecular cloud this idea appears untenable. We must note that this kind of problem has not been addressed in papers invoking this explanation, which also do not include the effects of explosive nucleosynthesis (see, e.g., Gounelle & Meynet 2012) and do not consider other crucial SLRs, like ^{135}Cs and ^{41}Ca. The very short-lived ^{41}Ca in particular would be completely extinct, in contrast with the striking correlation with ^{26}Al shown in Figure 1, which says it must have a stellar origin. Furthermore, these models assume that the WR star itself does not make significant further contributions to nucleosynthesis, in addition to those from the wind. This is not supported by other works (Higdon et al. 2004). In any case, all the results on the addition of SN debris, including ours, are somehow biased by oversimplifications in the treatment of the mechanism for the injection of fresh material, whose consequences still deserve detailed hydrodynamical studies of the type attempted by Boss (2017) and by Dwarkadas et al. (2017), but extended to all the measured SLRs.

On the other hand, the alternative origin in a (longer-living) AGB star, suggested early on by Wasserburg et al. (1994, 1995) for several radioactivities, has the weakness of requiring a chance stellar encounter at a level of probability that approaches zero (Kastner & Myers 1994).

Despite the criticisms, it is clear that a considerable number of radioactive nuclei among those in Table 1 must be of stellar origin and cannot be attributed to endogenic phenomena in the solar nebula itself—e.g., spallation processes induced by the solar wind (Sossi et al. 2017). In this respect, it is remarkable that the original suggestions by Wasserburg et al. (1994) on a possible AGB star origin, later specified by Busso et al. (2003) and Wasserburg et al. (2006), were subsequently and independently confirmed by Trigo-Rodríguez et al. (2009) on the basis of models for slightly more massive stars hosting hot bottom burning (HBB), i.e., hydrogen burning directly at the base of the convective envelope. In both these approaches it was assumed (with no real proof) that the parent star could produce elements from slow neutron captures (*s*-processes) only through the ^{22}Ne(α, n)^{25}Mg source, avoiding the formation of the complementary and rather efficient source ^{13}C(α, n)^{16}O. Even the AGB models, therefore, did not come without drawbacks that went beyond their implausibility. They were, however, not a priori excluded only because of their apparent success in accounting contemporarily for several SLRs (^{26}Al, ^{60}Fe, ^{107}Pd, ^{135}Cs, ^{182}Hf, ^{205}Pb).

In recent years, the abundance measurements of stable isotopes in pristine meteorites have been enormously improved, so that any possible scenario for an SN origin of SLRs must now face more stringent constraints than envisaged by Wasserburg et al. (1998). On the other hand, stellar models for both MSs and AGB giants have also undergone important improvements. We now have safe predictions of nucleosynthesis from CCSNe, which include rotation in the hydrostatic phases and a full computation of explosive nucleosynthesis (Chieffi & Limongi 2013, 2015). For smaller masses ($M \lesssim 8$–$9\,M_{\odot}$) attempts have been presented to address quantitatively, on the basis of known physical principles, the mixing of protons from the envelope into the He shell, which is preliminary to the activation of the reaction ^{13}C(α, n)^{16}O and the subsequent *s*-processing. These new kinds of models will be used here, in an attempt to limit free parameterizations and obtain more secure indications. The same will be done for MSs, adopting the mentioned computations where rotation and explosive phases are included. On these bases we shall also comment on scenarios for the evolution of a presolar molecular

cloud contaminated by a series of SN explosions and/or WR stars.

Before performing such a reanalysis, in Section 2 we present an update on the constraints that astrophysical models must face in terms of limits to the isotopic anomalies that nucleosynthetic events can introduce into the solar nebula, without violating accepted measurements. Subsequently, Section 3 briefly outlines the contributions to SLRs qualitatively expected to come from the uniform evolution of the Galactic disk before the formation of the Sun, showing that such a mechanism might account for most nuclei with a lifetime longer than about 5 Myr. Here we shall make some distinction between nuclei coming from relatively understood phases of stellar evolution and others produced in the very complex and still incompletely known process of fast neutron captures. We shall then outline a minimal summary of (some of) the complexities of this last process in Section 4, trying to make clear what kinds of characteristics are needed to account for ESS measurements. In particular, in Section 4.2 we show how certain neutron star merger (NSM) models, confirmed by some recent observations, might offer a way out for the longstanding problems associated with the ESS abundances of SLRs, especially in the case of nuclei like ^{129}I and ^{182}Hf. Subsequently, Section 5 illustrates possible contributions from a late-AGB star polluting the ESS. This is done with reference to recent models for partial mixing connected with the production of both ^{26}Al and the neutron source ^{13}C for *s*-processing. We focus in particular on two recent suggestions for the physical causes of these mixing processes, and for each of them, we show the predictions for the ESS radioactivities (in Sections 5.1 and 5.2). Then, we underline problems that were not yet clear at the time of publication of previous studies in this field. Subsequently, Section 6 examines the situation for a late contamination by an MS, while also briefly commenting on models of the sequential pollution of a presolar molecular cloud, which call in different ways for a role by MSs. Even in this case, the risks of encountering unsolvable problems are underlined. Finally, Section 7 draws some preliminary conclusions, discussing the parameter space that remains to be explored for attempting an explanation of the very puzzling problem of extinct solar system radioactivities.

2. Constraints from Isotopic Anomalies in Meteorites

As was first indicated several years ago (Wasserburg et al. 1998), an SN origin for SLRs present in the ESS would also necessarily introduce in the parent nebula variations over the pre-existing record of abundances for stable isotopes. In case the mixing is not homogeneous, this might imply the prediction of unobserved isotopic anomalies in elements typically produced by CCSNe. Any model of solar contamination in SLRs by MSs ending their evolution as CCSNe with inhomogeneous and clumpy ejecta must come with the guarantee that abundance shifts introduced in the stable isotopes of major elements remain at a level low enough not to be in conflict with actual measurements.

In ancient meteorites, variations in the isotopic composition of oxygen (the most important product of SN nucleosynthesis) are rather large. However, they are most likely mainly the result of chemical processes and self-shielding in the solar nebula (Clayton 2003) and not fingerprints of distinct nucleosynthetic components. More specifically, the O-isotopic ratios of bulk chondrites vary by about 10‰ amu^{-1}. Could this have an astrophysical origin—e.g., could it be the result of different abundances of presolar grains? The answer is no, as the most primitive meteorites have abundances of presolar O-rich grains of up to 500 ppm, which, with the typical ^{17}O enrichment of a factor of 2 in presolar grains, would shift the ^{17}O/^{16}O ratio by only 0.5‰ on a bulk scale.

Larger anomalies as compared to those in bulk chondrites are seen in specific components; notably, the most extreme cases are CAIs, with their enrichments in ^{16}O of up to 5%, as similarly inferred for the Sun by the *Genesis* mission (McKeegan et al. 2011) and for the so-called cosmic symplectite (formerly known as "new PCP"), which shows enrichments in ^{17}O and ^{18}O of up to 20% and which is assumed to represent primordial water in the solar nebula (Sakamoto et al. 2007). *Genesis* data suggest that CAIs have inherited mainly the O-isotopic composition of the gas in the solar nebula. Mixing the ^{16}O-rich gas of the ESS with ^{16}O-poor primordial water components in various proportions, along with mass fractionation effects, could easily account for the variations in O-isotopic composition of planetary materials, and there is no need to invoke a distinct nucleosynthetic component.

Much smaller isotopic variations are seen for heavier elements on a bulk meteorite (planetary) scale, some of which may be of nucleosynthetic origin. For the rock-forming elements Mg, Si, and Fe, isotopic anomalies are only at the sub–per mill level (Dauphas et al. 2017; Poitrasson 2017; Teng 2017). The same holds for many others of the heavy elements on a bulk meteoritic scale (Dauphas & Schauble 2016). Interestingly, relatively large Si-isotopic anomalies (with large experimental uncertainties) were found by the *Rosetta* mission for the refractory Si component in comet 67P/Churyumov–Gerasimenko, which has $\delta(^{29}\mathrm{Si}) = (-145 \pm 98)‰$ and $\delta(^{30}\mathrm{Si}) = (-214 \pm 115)‰$. Note, however, that here errors are at 1σ, so that within 2σ the composition would be normal (Rubin et al. 2017).

In conclusion, on a bulk meteorite scale there is no unambiguous evidence for isotopic anomalies of nucleosynthetic origin in excess of one per mill. Of course, if we include CAIs, especially FUN (and hibonite) inclusions, as references, things get much more complicated. A useful compilation of isotope data for conventional CAIs and FUN (and hibonite) inclusions can be found in Dauphas & Schauble (2016). For CAIs, isotopic anomalies of likely nucleosynthetic origin may reach up to a few per mill *for certain isotopes*, and for FUN (and hibonite) inclusions anomalies can be even much larger, in excess of a percent. However, we are looking for widespread, global signatures, while FUN inclusions are rare and exhibit strong mass fractionation effects. We believe they can be ignored in the present context, and we can consider only conventional CAIs along with meteoritic bulk composition. For them, isotopic anomalies of putative nucleosynthetic origin are clearly much lower on this scale.

As a conclusion, we must verify that in case the (typically clumpy and inhomogeneous) CCSN ejecta are assumed to be the source of SLRs in the solar nebula, the predicted shifts in the abundances of stable isotopes remain safely below the level of a few per mill. Only when the above constraints are verified can one consider nucleosynthetic processes in a close-by star as a possible origin for radioactive nuclei in the protosolar cloud.

Table 2
SLRs as Synthesized by a Uniform Production Model over $T = 10^{10}$ yr of Galactic Evolution

Rad.	Ref.	τ_R (Myr)	$[P^R/P^S]_{CE}$	$[N^R/N^S]_0$	$[N^R/N^S]_{10}$	$[N^R/N^S]_{20}$	$[N^R/N^S]_{Meas.}$
^{26}Al	^{27}Al	1.03	$5.4 \cdot 10^{-3}$	$5.6 \cdot 10^{-7}$	...	...	$(5.23 \pm 0.13) \cdot 10^{-5}$
^{41}Ca	^{40}Ca	0.15	$1.4 \cdot 10^{-3}$	$2.2 \cdot 10^{-8}$	...	...	$4 \cdot 10^{-9}$
^{53}Mn	^{55}Mn	5.3	0.189	$1.0 \cdot 10^{-4}$	$1.5 \cdot 10^{-5}$	$2.2 \cdot 10^{-6}$	10^{-6}
^{60}Fe	^{56}Fe	3.75	$2.3 \cdot 10^{-3}$	$8.0 \cdot 10^{-7}$	$5.6 \cdot 10^{-8}$	$3.8 \cdot 10^{-9}$	10^{-8}–10^{-6}
^{107}Pd	^{108}Pd	9.4	0.66	$6.2 \cdot 10^{-4}$	$2.1 \cdot 10^{-4}$	$7.4 \cdot 10^{-5}$	$(5.9 \pm 2.2) \cdot 10^{-5}$
^{129}I	^{127}I	23	1.30	$3.0 \cdot 10^{-3}$	$1.9 \cdot 10^{-3}$	$1.3 \cdot 10^{-3}$	10^{-4}
^{135}Cs	^{133}Cs	3.3	0.724	$2.1 \cdot 10^{-4}$	$1.0 \cdot 10^{-5}$	$4.9 \cdot 10^{-7}$	$4.8 \cdot 10^{-4}$
^{146}Sm	^{144}Sm	148	0.675	$9.9 \cdot 10^{-3}$	$9.2 \cdot 10^{-3}$	$8.6 \cdot 10^{-3}$	10^{-2}
^{182}Hf	^{180}Hf	12.8	0.346	$4.5 \cdot 10^{-4}$	$2.1 \cdot 10^{-4}$	$9.4 \cdot 10^{-5}$	$(9.81 \pm 0.41) \cdot 10^{-5}$
^{247}Cm	^{235}U	23	3.95	$8.9 \cdot 10^{-3}$	$5.8 \cdot 10^{-3}$	$3.7 \cdot 10^{-3}$	$(1.1–2.4) \cdot 10^{-3}$
^{205}Pb	^{204}Pb	22	1.05	$2.3 \cdot 10^{-3}$	$1.5 \cdot 10^{-3}$	$9.3 \cdot 10^{-4}$	10^{-3}

Note. Production factors from Wasserburg et al. (2006).

3. Contributions from Galactic Evolution

For a zero-order estimate of the contributions to SLRs from Galactic evolution, we consider a schematic model of an ISM behaving as a closed box enriched over a time duration T, following the approach by Wasserburg et al. (2006) and Lugaro et al. (2014). Then, the inventory of a radioactive isotope R relative to a stable nuclide S produced in the same astrophysical site at the moment production previous to the solar system formation ceases is

$$[N^R(T)/N^S(T)]^0_{CE} \simeq \frac{P^R p(T) \tau_R}{P^S \langle p \rangle T}, \quad (1)$$

where CE means chemical evolution, the superscript 0 indicates that the estimate is for the moment at which nucleosynthesis ceases, $P^S\langle p\rangle$ is the *average* stellar production rate of the isotope S over the time interval T, and $P^R p(T)$ is the production rate of R at the moment the process ends. Whenever $p(T)$ can be considered constant ($\simeq\langle p\rangle$), with Δ denoting the delay from the last nucleosynthetic episode after which the Sun forms, one has

$$[N^R(T)/N^S(T)]^\Delta_{CE} \simeq \frac{P^R}{P^S} \cdot \frac{\tau_R}{T} \cdot e^{-\Delta/\tau_R}. \quad (2)$$

A problem with this treatment is that we need to apply it to nuclei produced by heterogeneous sources, e.g., by hydrostatic and explosive processes in stars of different mass and by slow and rapid neutron captures. For the latter, Wasserburg et al. (1996, 2006) started simply from the assumption of the existence of a unique explosive scenario capable of reproducing the solar system distribution of *r*-nuclei and derived the production ratios accordingly. Although in Equation (2) we now need only such ratios (P^R/P^S) for isotopes of the same element that are very close in mass, the problem of connecting the data for nuclides having different origins (e.g., ^{53}Mn, the *p*-nucleus ^{146}Sm, the *s*-process nucleus ^{205}Pb, or the *r*-nucleus ^{247}Cm) remains, so that the results of Galactic enrichment are affected by intrinsic strong uncertainties and must be considered with much caution.

Should one accept the indications by Wasserburg et al. (2006), one would find that the ratio P^R/P^S is close to 1 for ^{107}Pd, ^{129}I, and ^{135}Cs (0.66, 1.3, and 0.724, respectively). This ratio is much lower ($\simeq 1.4 \cdot 10^{-3}$) for ^{41}Ca. Also, for ^{26}Al the production ratio to ^{27}Al is low. For example, in SNe and MSs P^R/P^S is expected to be between 10^{-2} and 10^{-3}; the adopted average value then is $5.4 \cdot 10^{-3}$. This last estimate might be suitable for explaining the Galactic inventory of ^{26}Al ($2.8 \pm 0.8\,M_\odot$; see, e.g., Diehl et al. 2006). This corresponds to an average ratio ^{26}Al/^{27}Al of a few 10^{-6}, which is one-tenth of the ratio for the ESS (see also Higdon et al. 2004). For ^{60}Fe, the adopted production ratio to ^{56}Fe is $2.27 \cdot 10^{-3}$, and for Hf, $P^{182}/P^{180} \simeq 0.346$. Table 2 gives a synthetic view of the abundance ratios that can be obtained with these hypotheses, either at the moment when nucleosynthetic episodes preceding the solar formation ceased ($\Delta = 0$) or after a delay of the order of the isolation times of cloud cores in star formation regions (Δ of up to (1–2) $\cdot 10^7$ yr).

The above general picture does not really aim (and never did aim) to be quantitative, both for uncertainties in production factors in stars and for the extremely elementary scheme of chemical evolution adopted for the Galaxy. It is only a general qualitative view to be improved by future models. In this respect, we cannot aim (in such a rough picture) to obtain agreement with measurements at levels better than a factor of 2–3; this is a minimum estimate for the uncertainty in the scheme adopted. Especially for Galactic evolution one should actually consider more sophisticated models—e.g., those in Mathews et al. (2014), Bojazi & Meyer (2017, 2018), and Dwarkadas et al. (2017).

Nevertheless, the above picture already provides relevant pieces of information. It turns out that nuclei of very different origins, like ^{53}Mn, ^{107}Pd, ^{146}Sm, ^{182}Hf, ^{205}Pb, and ^{247}Cm, might actually find a proper explanation for an isolation time between 10 and 20 Myr. Even the very uncertain ^{60}Fe might not be a problem, in case the most recent estimates for its abundance are confirmed (Trappitsch et al. 2018). The nuclides that are clearly underproduced by this simple and expected process of gradual Galactic enrichment are only limited to ^{26}Al, ^{41}Ca, ^{135}Cs, and possibly ^{60}Fe (the latter only in case its initial ESS ratio to ^{56}Fe should turn out to be higher than 10^{-7}).

However, in the case of heavy *n*-rich SLRs, the situation is more complex, as pointed out early on by Cameron et al. (1993) and Wasserburg et al. (1996). Here one has to consider, aside from the *s*-process nuclide ^{205}Pb, isotopes of possibly heterogeneous origin, like ^{107}Pd, ^{182}Hf, ^{247}Cm, and others, including ^{129}I, due to the *r*-process. While the stellar yields of slow neutron capture nuclei are rather well understood, the situation is quite different for *r*-process isotopes, whose origin is not yet quantitatively established. SLRs make clear that ascribing them to a unique mechanism taking place in some explosive event of a non-specified nature, as is done in Table 2, implies enormous overproductions for ^{129}I with respect to

^{107}Pd, ^{182}Hf, and ^{247}Cm; hence the works by Cameron et al. (1993) and Wasserburg et al. (1996) simply noted that such a unique scenario was unlikely. Understanding heavy SLR abundances now, some 25 years later, requires placing them in the broader context of more recent observations and models for the *r*-process. We shall try to discuss these issues in the next section.

4. Constraints and Models for *r*-process Nucleosynthesis

4.1. Observed Constraints and r-process Sources

In the *average* solar system abundances, the decay daughters of ^{129}I and ^{182}Hf have a ratio of $N(^{129}\mathrm{Xe})/N(^{182}\mathrm{W}) = 41.6$ (Lodders & Palme 2009); as ^{182}W is of *r*-process origin only for about 50% (Trippella et al. 2016), the abundance ratio between the *r*-components of these nuclei should be slightly higher than 80. Should we adopt the *s*- and *r*-components from Bisterzo et al. (2014), we would get a higher estimated ratio of 114. In contrast, in the ESS, given the fact that the isotopic ratios $^{129}\mathrm{I}/^{127}\mathrm{I}$ and $^{182}\mathrm{Hf}/^{180}\mathrm{Hf}$ are essentially equal ($\simeq 10^{-4}$), the ratio between the two SLRs roughly equals that of the stable references, i.e., $^{127}\mathrm{I}/^{180}\mathrm{Hf}$, which is about 20. There is a discrepancy of about a factor of 4. With respect to the rough predictions of Table 2, referring to the continuous Galactic production of *r*-process nuclei from hypothetical sources of a unique nature, the discrepancy reaches up to a factor of 7–10 (see columns 6 and 7). This sharp contrast might probably be accounted for only if the two cases (the average solar system materials and anomalies in early solids) derive from different origins or different admixtures of *r*-process "components." In particular, the average solar system abundances were built through an elaborate blend of different processes, each accounting for one such "component" of the distribution. This blend was established by Galactic evolution over a timescale of $\simeq$10 Gyr. SLRs in the ESS produced through fast neutron captures might instead evidence the granularity of the Galactic mechanism on shorter timescales, possibly being controlled by only a few contributions from specific sources (Cameron et al. 1993).

Wasserburg et al. (1996) tried to infer the origins of the above contributions; although the reference sources then were mainly assumed to be CCSNe, through neutron captures occurring in a neutrino-driven wind (Woosley et al. 1994), this assumption actually does not enter directly into the estimates of Table 2, which simply require a single mechanism reproducing the solar *r*-process abundances. The same approach was discussed by Busso et al. (1999). As a simple recipe for finding a way out, Wasserburg et al. (1996) guessed that the astrophysical source for the production of ^{129}I appeared for the last time in the solar neighborhood a long time before the last event producing ^{182}Hf and ^{247}Cm, thus implying a much longer decay of the first one, from which the low ESS ^{129}I abundance would derive. This was subsequently extrapolated by Qian & Wasserburg (2000), who assumed more explicitly a specific source for these nuclei (CCSNe) and proposed that two types of these were at play, one producing the lighter *r*-nuclei, up to $A \simeq 130$ (including iodine), and the other producing the heavier nuclei. The first kind of events was indicated with the letter *L* (*lower*, from their low expected rate of occurrence), and the second was indicated with *H* (*higher*). ^{107}Pd would be low in that hypothesis, but for it the *s*-process can be invoked (see Section 5).

The above ideas generated extended debates and were in general criticized as being simplistic. It was in particular underlined that, within CCSN models for the *r*-process, any *physically based* mechanism yielding enough ^{182}Hf to explain its ESS abundance would most probably also produce the nuclei at the $N = 82$ peak, including ^{129}I, thus leading to high values of their ratios (see, e.g., Pfeiffer et al. 2001). In other words, the requirement of having "pure" *r*-process sources separately producing the two nuclei seemed to be too ad hoc to be accepted. More plausible might be situations where they are produced together but at different efficiencies. For example, this would be the case—using a rather recent mass model, like the finite-range droplet model update by Möller (2012)—if a weakening of the $N = 82$ shell closure (often referred to as "shell quenching") were to occur below the doubly magic ^{132}Sn (Dillmann et al. 2003; Atanasov et al. 2015). This would anticipate the maximum of the peak, perhaps down to $A =$ 126 (see Table 1 in Kratz et al. 2014a). Then ^{129}I would not stay at the peak, but after it, with a reduction of its abundance by a factor of 2−3 with respect to a standard solar *r*-component (Farouqi et al. 2010).

Subsequent research then clarified that other sources, different from CCSNe, might be crucial in producing *r*-process nuclei (Freiburghaus et al. 1999). At the time of writing, two main sites have often been discussed to have excellent chances to contribute, in various proportions, to producing nuclei from fast neutron captures. They are the rare magnetorotational types of SNe (MRSNe; see, e.g., Nishimura et al. 2017 and references therein) and NSM events (see, e.g., Freiburghaus et al. 1999). One has to mention in particular that this last paradigm received a now popular observational support in the recent gravitational-wave event GW 170817 (Abbott et al. 2017). In the electromagnetic source AT 2017gfo, the kilonova associated with it, qualitative evidence has been recorded of the production of heavy *n*-rich elements at the second or third abundance peak (Pian et al. 2017; Tanvir et al. 2017; Troja et al. 2017). The possibility of having *r*-process nucleosynthesis in such an environment was suggested early on by Lattimer et al. (1977), Meyer (1989), and Eichler et al. (1989). This kind of model was recently suggested to be in principle able to explain the whole solar system distribution of nuclei coming from fast neutron captures (Wanajo et al. 2014; Thielemann et al. 2017). One also has to consider cautiously that the traditional CCSN models seem not to be completely out of the picture yet (Kajino & Mathews 2017). There has also been persistent speculation that CCSNe of a specific type (faint, ^{56}Ni-poor type-IIP events showing enhanced Sr II and Ba II lines, like SN 2009E and perhaps SN 1987A; see, e.g., Pastorello et al. 2012) can contribute to the *r*-process, as suggested early on by Tsujimoto & Shigeyama (2001). Although the strength of Ba II lines might be affected by variable ionization and temperature issues (Utrobin & Chugai 2005; Pastorello et al. 2012), these effects should be valid in general and might not explain completely why in other CCSNe the Ba and Sr lines are significantly weaker (Branch & Wheeler 2017). The products of the above faint SN II sources might have been observed in dwarf galaxies (Ji et al. 2016a). In general, the real relative importance of the various contributors to heavy neutron capture nuclei, their frequency of occurrence,

and the amount of processed material returned to the Galaxy remain uncertain, although NSMs, where large neutron excesses are found, are emerging as some of the most promising sites for *r*-processing (Thielemann et al. 2018).

Constraints on the zoo of present-day models can be found by considering real observed or measured element admixtures (Kratz et al. 1993). In our case, these include not only the solar system average abundances and ESS radioactivities but also the pattern of *r*-nuclei observed at low metallicity in our Galaxy and its neighbors when the *s*-process has not yet started to appear and one has chances to see stars polluted by only part of the long-term *r*-process blend (Sneden et al. 2008). In this framework, it has by now been ascertained that many old stars exist showing an almost solar distribution of elements across and beyond the $N = 82$ magic neutron number (Spite et al. 2018). The prototype of these objects is the famous CS 22892-0052 source (Sneden et al. 1996), a supergiant in Aquarius. When in these stars one also considers lighter species (with $Z = 40$–50), one sees that their scatter is large, but on average the production of these elements is lower by a factor of 2–3 with respect to a scaled solar *r*-process distribution (see, e.g., Honda et al. 2006, particularly their Figure 5). Completely different metal-poor stars, however, exist at even lower metallicity, the prototype being the subgiant/giant star HD 122563 (Honda et al. 2006). Here, the light *r*-nuclei at $N = 50$ are dominant with respect to heavier species across and beyond the $N = 82$ peak. We further note that the inventory of low-metallicity stars differently enriched in *light* and *heavy* *r*-nuclei seems to suggest that the former ones are actually more frequent than the latter ones and that the amount of *r*-processed matter ejected by events producing the lighter *r*-process elements is much smaller than the amount ejected by those preferentially producing the heavier nuclei, approximately by two orders of magnitude (Macias & Ramirez-Ruiz 2016). The two producing environments might be of heterogeneous origin (e.g., CCSNe and NSMs) or of the same type (e.g., NSMs only), but occur in different conditions. For example, it has been shown that NSM phenomena can give rise to light or heavy *r*-nuclei, depending on the extremely variable possible conditions. At any rate, deriving absolute production factors, like the $\langle p \rangle$ values needed in Equation (1), is certainly premature, so that we are obliged to stay at a purely qualitative discussion. Moreover, both HD 122563 and CS 22892-0052 reflect situations probably not suited to explain the ESS ^{129}I/^{182}Hf ratio. Although the most relevant elements—I, Xe ($Z = 53$–54) and Hf, W ($Z = 72$–74)—were not observed, looking in general at the closest elements we see that, from both cases, we would expect a ratio much higher than that observed in the ESS. Hence, if this last sample reflects the isotopic ratios typical of a specific *r*-process variety, then the two types of metal-poor stars (albeit offering a closer and different look at the granularity of the process) should already be the products of different forms of admixtures of heterogeneous components.

Albeit with caution, we can say that something better, more similar to the individual *r*-components revealed by ESS heavy SLRs, may actually exist in some metal-poor stars. A few years ago it was shown, in Roederer et al. (2016), that three out of four stars observed in the dwarf galaxy Reticulum 2, although generally similar to Sneden's Star, actually show rather high abundance ratios between the heavy elements before the third *r*-process peak (e.g., Dy) and those immediately after the second peak (e.g., Ba). In the mentioned stars the ratio Dy/Ba ranges from 7 to less than 24 (upper limit) times the average solar value. This value needs to be corrected for deriving a pure (solar) *r*-process component. This can be done using the *r*-residuals (1-*s*) from the models quoted in the next section, particularly those from Palmerini et al. (2018). With respect to previous computations, these models yield lower estimates for the Dy_r/Ba_r ratio in the Sun, in the range 2.7–5, with an average value depending on the initial mass function adopted for the weighting, on the mass loss rates, etc. One can roughly evaluate it to be near 3.5 (against a previous estimate of 5.7, derived from Bisterzo et al. 2014). We underline that the new estimates are quite uncertain; despite this, they are closer to what can be found in high-entropy wind (HEW) models with shell quenching (see e.g., Farouqi et al. 2010), where values down to 2.0−2.3 can be obtained. With the above correction (on average by a factor of 3.5) for the solar *r*-component normalization, the Dy/Ba ratios in the three stars of Reticulum 2 become 2, 4.5, and less than 6.8 (upper limit) times as high as those in the solar *r*-process distribution. Can one roughly assume that this also implies relatively high ratios near (the unobserved) W and Xe (whose isotopes at $A = 182$ and $A = 129$ are decay daughters of the SLRs we are discussing)? As we have illustrated, we need an enhancement factor in ^{182}Hf/^{129}I of about 4; if our extrapolation is correct, the early observations of Reticulum 2 showed real stars where this might be achieved. A similar situation may apply to the more numerous stars recently observed by Hansen et al. (2018). In their Table 5, several measurements identify objects (called *r*-I) with negative values of Eu/Ba; some of them yield linear Ba/Eu ratios lower than those in the solar *r*-distribution. Models accounting for this trend include the mentioned HEW cases with shell quenching and certain NSM scenarios, e.g., those by Goriely et al. (2013). Hence, two different sites, affected by *r*-process varieties similar to the one producing the heavy SLRs, would have been observationally confirmed. At present, NSMs seem to be the most probable sources to explain the above abundance distributions, due to their lower Y_e values with respect to CCSNe.

In any case, the abundance distributions of different metal-poor stars confirm that various *r*-process varieties must necessarily exist and that the blend shown by the average solar composition is certainly not "universal," as also indicated by the extensive theoretical work of the last 25 years (see, e.g., Roederer et al. 2010; Kajino & Mathews 2017; Tsujimoto et al. 2017; Thielemann et al. 2018; and references therein).

With the above scenario in mind, one can look for parameter studies based both on site-independent and on site-specific models to identify the astrophysical conditions required for reproducing observational evidence. From these conditions we can then try to figure out plausible scenarios accounting for the abundances of ^{129}I and ^{182}Hf in ESS samples without violating other constraints from low-metallicity stars.

4.2. Reconciling the ESS Abundances of ^{129}I and ^{182}Hf

It is generally recognized that a very promising general scheme for *r*-processing involves neutrino-driven interactions in neutrinospheres and/or neutrino winds (NWs) established in explosive conditions above a neutron star (Freiburghaus et al. 1999). These might be found in various astrophysical scenarios (CCSNe, NSMs, MRSNe; see, e.g., Kajino & Mathews 2017).

A few works some years ago criticized earlier attempts aimed at modeling their occurrence in CCSNe (see, e.g., Fröhlich et al. 2006; Wanajo & Janka 2012), inferring that, for those conditions, the NW would remain proton-rich during its entire life, precluding any *r*-process nucleosynthesis, even simply for producing light nuclei up to the first magic neutron number, $N = 50$ (Sr, Y, and Zr). However, Roberts et al. (2012) re-established this scenario as a possible one for the occurrence of neutron captures. They showed that, with a more detailed treatment, including the nucleon potential energies and the collisional broadening of the response, the previous negative conclusions would be considerably changed. In particular, for a reasonable period of time, the NW was predicted to remain moderately neutron-rich. Interactions occurring in the NW have been described, e.g., in Ott & Kratz (2008), Farouqi et al. (2010), Martínez-Pinedo et al. (2017), and Thielemann et al. (2018). The main parameters controlling the nucleosynthetic products are the number of neutrons per nucleus $Y_n/Y_{r\text{-seed}}$, the number of electrons Y_e, the expansion velocity $v_{\rm exp}$, and the entropy per nucleon S (generally expressed in units of Boltzmann's constant $k_{\rm B}$). They are linked by the relation (Farouqi et al. 2008a, 2008b; Kratz et al. 2008)

$$Y_n/Y_{r\text{-seed}} \simeq v_{\rm exp} \cdot \left(\frac{S}{Y_e}\right). \quad (3)$$

In CCSNe only limited neutron enrichments seem to be achieved ($Y_e = 0.4$–0.45); to produce heavy nuclei requires high values of the entropy per nucleon S to be available ($S \geqslant 200$), which gives the mechanism its denomination: HEW. Nucleosynthesis induced by neutrino interactions can also occur in contexts different from CCSNe, particularly in NSMs, where the neutron excess is always much larger (with Y_e values down to 0.2); there, lower values of the entropy S are required ($S \lesssim 20$; *low-entropy winds*). These are some of the reasons why so much attention has been dedicated to this scenario in recent years.

In the original work by Roberts et al. (2012) the values of Y_e and the maximum entropy $S_{\rm Max}$ for CCSNe were such ($Y_e \simeq 0.45$, $S_{\rm Max} \leqslant 100$) that only relatively light trans-Fe elements, from Sr to maybe Ru, could be produced in a process with high proton abundance. A result of this kind had been previously discussed by Farouqi et al. (2009), in addressing the composition of presolar SiC grains of type "X" (Pellin et al. 2006).

However, following that report by Roberts et al. (2012), a few groups showed that in some scenarios HEW models could still apply, reaching high values of $S_{\rm Max}$ (Kratz et al. 2014b; Thompson & ud-Doula 2018). According to them, this is a necessary condition for the process to be effective at relatively high Y_e values, as in CCSN contexts. For example, explaining with these sources observations of extremely metal-poor stars, like HD 122563 (Honda et al. 2006), with ejecta from a moderately neutron-rich wind ($Y_e = 0.45$, as in Roberts et al. 2012) would require $S_{\rm Max} \simeq 220$. Should one try to account for other metal-poor stars richer in heavy *r*-nuclei, like CS 22892-0052 (Sneden et al. 2008), in the same $Y_e = 0.45$ condition, $S_{\rm Max}$ as high as 280–300 would be needed (Farouqi et al. 2010; Kratz et al. 2014b). If, instead, the game is played in more *n*-rich environments, like NSMs, these requirements would be reduced by roughly a factor of 10 (Thielemann et al. 2017).

One also has to note that virtually any observed star, even at very low metallicity, contains an admixture of light and heavy *r*-nuclei. As an example, *r*-poor stars, like HD 122563, have Sr/Eu values of about 100 to about 550, whereas *r*-enriched stars, like CS 22892-0052, have Sr/Eu ratios of about 20 to about 30. Recent extreme cases were shown by Ji et al. (2016b) for stars enriched in heavy ($A > 130$) nuclei; they have Sr/Eu ratios lower than 10, down to a minimum of about 3.5. If these numbers define a pure "main" *r*-component, then all other observed stars contain admixtures of different processes, i.e., they are characterized by wider blends of Y_e and S values than obtained in individual calculations (Frebel & Beers 2018). This is so even at very low metallicities ([Fe/H] $\lesssim -2.5$), where the stars should have been polluted by only very few SN events. If NSMs are at play, their potentially much lower Y_e values would allow all *r*-nuclei up to the heaviest ones to be produced in rather low-entropy conditions (Goriely & Janka 2016; Thielemann et al. 2018).

In general, what we expect as a result of NW-driven nucleosynthetic phenomena for increasing values of $S_{\rm Max}$ can be outlined as follows.

1. In CCSNe, for the lowest values of $S_{\rm Max}$, a primary-like, rapid nucleosynthetic process can start in the dynamics of the mechanism, mainly controlled by charged particle interactions, where Y_n/Y_r is lower than unity. In these conditions SiC grains of type "X" might find their production site (Pellin et al. 2006; Farouqi et al. 2009). This requires $S_{\rm Max}$ to be up to 100 for typical Y_e values of 0.45 (Farouqi et al. 2009). This condition is not met in NSM environments, where the material is always neutron-rich.
2. For increasing values of $S_{\rm Max}$ and Y_n/Y_r, neutrons start to dominate, and we find various rapid *n*-capture processes. These variants have been called *weak*, *incomplete*, or, for higher S values, *main* and *actinide-boost* *r*-processes. Typically, the same regions of A can be reached in NSM models for S values smaller by an order of magnitude, due to the generally much lower Y_e.
3. In CCSNe, for values of $S_{\rm Max}$ around 150 and of free-neutron abundances in the range $1 \lesssim Y_n/Y_r \lesssim 15$ one would find what is called by stellar modelers the "weak" *r*-process. Although light *r*-nuclei are produced, these are not the conditions for explaining the star described by Honda et al. (2006), as this star includes some heavy nuclei, while here production stops at the rising wing of the $A = 130$ peak, producing iodine at a low level of a few percent. Similar results can be obtained with NSM models at values of $S_{\rm Max}$ up to one-tenth of the above value (Siegel & Metzger 2017).
4. There might be a following, more effective *r*-process mechanism for larger values of Y_n/Y_r and for $S_{\rm Max}$ values ranging between 200 and about 220 in CCSNe (again smaller by an order of magnitude in NSMs, with Y_e values smaller by typically a factor of 2). Its existence is evidenced by stars where nuclei in the region from Sr to Cd dominate but are accompanied by variable abundances of heavier species, like Ba and Eu. Examples of such stars with a rather scattered composition are abundant. In addition to those cited by Honda et al. (2006), new measurements have been presented by Hansen et al. (2012). This has been called a "limited

r-process," repeating suggestions advanced by Roederer et al. (2010) and others.

5. A main *n*-capture mechanism follows, responsible for the top of the $A \simeq 130$ peak, including most of Xe, the rare earth elements, and the $A \simeq 195$ third *r*-peak. This process is often referred to as a "Sneden-like" *r*-process, as it would account for stars with a solar system distribution of elements above $A \geqslant 130$, like those described in Sneden et al. (2008), plus a variable proportion of lighter nuclei. This kind of process might occur in CCSNe for values of Y_n/Y_r up to about 150 and values of $S_{\rm Max}$ above 220. Again, in NSM scenarios suitable conditions require much smaller values of $S_{\rm Max}$, due to the low Y_e. In this process the enhancement factor for iodine would traditionally reach up to more than 90% of the most effectively produced elements, like Eu. However, its abundance can be considerably reduced if a weakening of the $N = 82$ shell closure (often referred to as "shell quenching") occurs below the doubly magic ^{132}Sn (Dillmann et al. 2003; Atanasov et al. 2015). This would anticipate the maximum of the peak, perhaps down to $A = 126$ (see Table 1 in Kratz et al. 2014a). In those conditions the ratio I/Hf would be considerably reduced. The same effect would also be obtained by further increasing $S_{\rm Max}$. Models of the *main* component with a low I/Hf ratio seem to also be possible in NSM models with high efficiency, e.g., those in Goriely et al. (2013), Goriely & Janka (2016), and Bauswein et al. (2013).
6. There might be a further, limited contribution from a very efficient *n*-capture process (that would explain the "actinide-boost" stars). Some of the stars observed by Roederer et al. (2009) might have these characteristics.

Depending on the ambient conditions, any site might be characterized by a specific range of *S* values. Their superposition, from many different events, gives rise to the robust distribution of *r*-process nuclei observed in young Galactic stars. In the specific case of the *main* component, nuclei with $A \geqslant 135$ and $Z \geqslant 56$ are produced with abundance ratios that are remarkably constant since their early appearance in low-metallicity stars (see, e.g., Sneden et al. 2008; Hill et al. 2017; and references therein).

We have then two possible ways out for the I/Hf ratio. On the one hand, the same *main* component might produce a much lower abundance of iodine than previously found in CCSN models. This is obtained in certain NSM scenarios producing rather heavy *r*-nuclei (Bauswein et al. 2013; Goriely et al. 2013) and might also be found in CCSNe, where very high entropies and shell quenching effects substantially reduce the previously expected I/Hf predictions. In both cases, the observed ESS ratios might be the direct outcome of only one specific *r*-process site, possibly the same one producing the abundance patterns observed in some halo stars by Hansen et al. (2018) and in Reticulum 2 by Roederer et al. (2016). In view of the fact that NSM models show a high number of free neutrons, this scenario is probably the most promising one for yielding the required ^{129}I/^{182}Hf ratio. Another variety of NSM phenomena, with a lower number of neutrons per seed, might then be at the origin of ^{107}Pd, in a weaker *r*-process. As mentioned, this *weak* component might also come from CCSNe in suitable conditions. Table 2 would still be broadly similar to reality, but the production factor $\langle p \rangle$ for ^{129}I should be reduced by a large factor, maybe of the order of 5 ($\pm$ a factor of 2, trusting the few data from Reticulum 2).

Alternatively, the ESS ^{129}I might derive from the averaging over timescales much shorter than 10 Gyr of the contributions from different sources: a very limited number of them with a *traditional* main *r*-mechanism and a much larger number with a *weak* mechanism, with poor efficiency (a few percent) in ^{129}I production. ^{182}Hf, instead, would be fully produced by the *main r*-process, with negligible contributions from the sources responsible for weaker components. In this second case, the production of I and Hf would be essentially decoupled; however, in that case we would have the problem of obtaining the correct relative efficiencies (in frequency and mass ejected) of different producing sites for explaining Pd, I, and Hf in an admixture of different sources. This seems a prohibitive fine-tuning task now; we therefore tentatively indicate the first possibility as the more probable.

We mention here that ^{182}Hf is well accounted for by the Galactic enrichment of *r*-process elements. We therefore do not feel any need to increase its *s*-process fraction, as done in Lugaro et al. (2014), following the revision of the level scheme and of the decay rate of ^{181}Hf, which ensues by a single estimate (Bondarenko et al. 2002). On this point we prefer to maintain a cautious approach, waiting for possible confirmations of this individual measurement.

5. The Reference Models for Intermediate-mass Stars (IMSs)

When a radioactive nucleus is not accounted for by the chemical evolution of the Galaxy and requires a late event of nucleosynthesis to explain its abundance in early solids of the solar system, a formalism slightly different from Equation (1) applies to it. As discussed in Wasserburg et al. (2006), if a nearby star produced a radioactive nucleus *R* of mean life τ_R, introducing for it in the ESS an abundance ratio $\alpha^{R,S}$ with respect to a stable isotope *S* of the same element, the following relation holds between the $\alpha^{R,S}$ value and the abundance ratio N^R/N^S (radioactive versus stable) in the stellar envelope:

$$\alpha^{R,S} = d \cdot \frac{N^R}{N^S} q^S e^{-\tau_R/\Delta}. \quad (4)$$

Here q^S is the enhancement factor of the stable isotope *S* in the same envelope. The parameter *d* represents a dilution factor that measures the fraction of the ejected wind that is incorporated into the forming solar cloud, while Δ has the same meaning as in Equation (2).

In considering the stellar sources suitable for a late contamination of the solar nebula with SLRs, in this section we start with an estimate of the possible role played by IMSs. This issue was recently addressed by Wasserburg et al. (2017). They assumed that below an initial mass of about 5 $M_\odot$ a ^{13}C pocket could be formed during the AGB phases, inducing the reaction ^{13}C(α, n)^{16}O and producing neutrons efficiently through it. Above this limiting mass they instead considered only neutrons from the ^{22}Ne(α, n)^{25}Mg reaction. These more massive models were found to experience HBB at the base of the convective envelope, efficiently producing ^{26}Al. Contrary to previous observations by Trigo-Rodríguez et al. (2009), those authors could not find an explanation for SLRs in their models. In the lower-mass range ^{26}Al was insufficiently produced with respect to *s*-elements; for the higher masses the reverse was true. They suggested that a compromise

solution might be found midway between the two cases, but did not present a detailed model for it. One notices that in these computations the ^{13}C source was introduced ad hoc and without a physical model for it, as was common in many computations of the last 20 years or so. Moreover, for HBB the model dependency is high, so that these calculations cannot be considered conclusive.

The approach we want to follow here is different. Whenever possible, we would like to base our considerations on physical models that avoid (as far as possible today) free parameterizations. This attempt must address first of all the chemical peculiarities of light elements and CNO isotopes observed in stellar photospheres (see, e.g., Gilroy 1989) and not directly accounted for by traditional stellar models. These peculiarities trace the existence, in stars below 7–8 $M_{\odot}$, of nonconvective transport phenomena. In particular, for low-mass red giants, several authors (see, e.g., Busso et al. 2010; Palmerini et al. 2017; and references cited therein) have shown that the known episodes of convective mixing that occur after the star enters its red giant branch (RGB) stage and that carry to the envelope materials previously processed by nuclear reactions are not sufficient to explain their isotopic abundance observations from ^{7}Li up to ^{26}Mg. The most important mixing episodes of this kind are the "first dredge-up" and the "third dredge-up" (hereafter, TDU). The first one is induced by the inward expansion of the envelope after the main sequence; in solar-metallicity stars its main effect is a reduction of the ^{12}C/^{13}C ratio at the start of the RGB stage to 25–30 (from the initial solar value around 90) and a contemporary increase of the ^{14}N surface abundance. The second mixing episode is a similar envelope penetration occurring repeatedly, after runaways of the He-burning shell called "thermal pulses" (TPs), during the final AGB phase. It mixes mainly helium, carbon, and *s*-process elements with the envelope. Stars more massive than about 2.2 $M_{\odot}$ also experience a "second dredge-up" (SDU) in early phases of the AGB, carrying up materials polluted by extensive H-burning processes, including He and ^{14}N. In Section 5.2 we shall see that further consequences of interest to the present study may also emerge.

For understanding the further mechanisms of mixing and nucleosynthesis that must be at play in evolved low-mass stars and IMSs, stellar spectroscopic data are crucially supplemented by the record of isotopic abundances accurately measured in presolar grains found in pristine meteorites, as most of these grains were actually formed in the circumstellar envelopes of AGB stars. Wasserburg et al. (1995) suggested that the peculiar isotopic composition of oxygen found in a large number of presolar corundum (Al_2O_3) grains could be explained assuming the presence of deep matter circulation in the mentioned stellar sources; the same process would also be responsible for the presence of ^{26}Al in some of these grains as well as for the high abundances of ^{13}C and the spread in the concentration of ^{7}Li observed in low-mass red giant stars. These suggestions were then confirmed by Nollett et al. (2003) and later by Palmerini et al. (2011a, 2011b).

Since then, several works have been presented by various groups to interpret those results, originally obtained with parameterized approaches, on the basis of models physically built on some fundamental properties of stellar plasmas. These properties ranged from rotational mixing (Charbonnel & Lagarde 2010) and thermohaline diffusion (Eggleton et al. 2006, 2008; Charbonnel & Zahn 2007) to asteroseismic effects inducing gravity waves (Denissenkov & Tout 2003) and transport guaranteed by the buoyancy of magnetic flux tubes (Busso et al. 2007). Later, some of these mechanisms were found to be too slow to induce remarkable effects on the RGB (or even on the shorter AGB phase); this was, for example, the case with thermohaline diffusion (Denissenkov & Merryfield 2011). The other mechanisms were not applied in detail to the interpretation of isotopic abundances on both the RGB and AGB and then compared to constraints coming from presolar grains.

Two remarkable exceptions, however, exist. On the basis of considerations concerning the physics of the inner border of the convective envelope of a red giant and the effects of rotation, Cristallo et al. (2009, 2011, 2015a, 2015b) performed a general revision of the models, both for low-mass stars ($M/M_{\odot} \lesssim$ 2–2.2) and for IMSs (2–2.2 $\lesssim M/M_{\odot} \lesssim$ 7–8). The effects of partial mixing were introduced along the whole evolutionary history and were extended to include the inner He-rich layers, where the presence of deep mixing (DM) phenomena causes the formation of a ^{13}C reservoir conducive to inducing the activation of a ^{13}C(α, n)^{16}O neutron source.

Independently of that, Nordhaus et al. (2008) and subsequently Nucci & Busso (2014) showed that the known mechanisms associated with magnetic stellar activity might induce circulations and transport phenomena in the external layer of a star that in specific circumstances might become quite fast (up to 100 m s^{-1}). Along the RGB and AGB sequences, their activation can carry materials modified by nucleosynthesis in H- and He-burning shells to the surface of the star. Detailed calculations of the consequences of such a suggestion were subsequently performed by Trippella et al. (2014), Wasserburg et al. (2015), and Trippella et al. (2016) and more recently by Palmerini et al. (2017, 2018), who compared the results with a series of constraints ranging from the solar system distribution of *s*-elements to the record of oxygen isotopic anomalies and of ^{26}Mg excesses induced by the in situ decay of ^{26}Al in presolar oxide grains and up to the isotopic admixtures of trace *n*-rich elements in presolar SiC grains.

In the following two subsections we shall briefly review what kinds of predictions for SLRs in the early solar nebula can be derived by assuming that the forming Sun was contaminated by slow winds of an AGB star of intermediate mass, hosting either of the two mentioned DM processes. The reference models we adopt have similar general input parameters. Those in Section 5.1 adopt the compilation by Lodders & Palme (2009) for scaled solar abundances and that by Dillmann (2014) for neutron capture cross sections. For the models in Section 5.2 the choices are Lodders (2003) and Bao et al. (2000); none of the small differences present in these databases has any effect on the results discussed here. In both cases, as mentioned previously, we do not adopt for ^{182}Hf the suggestions by Lugaro et al. (2014), indicating a revision of the decay rate for the precursor ^{181}Hf, which would substantially increase the *s*-process contribution to ^{182}Hf. This suggestion was based on a single measurement, and on the basis of our discussion in Section 3, this last SLR seems already well explained by the Galactic enrichment in *r*-process nuclei. We prefer in these conditions to cautiously wait for new experimental evidence.

5.1. Effects of a Late-AGB Star. I. Models with MHD-induced Mixing

Nucci & Busso (2014) demonstrated that the very complex MHD equations valid for a stellar plasma might be drastically simplified in some specific geometries well approximating the radiative layers below the convective envelope of an evolved star. In this particular case, the equations can be solved analytically in an exact way, yielding simple formulae that can be introduced into stellar models to mimic the local effects induced by the magnetic field. In particular, the solution refers to the general process of buoyancy of magnetized zones described by E.N. Parker in the fifties, leading to their emergence in the convective envelopes at a rather fast speed.

While this simple analytic solution to the MHD equations can be found under rather broad conditions, when we impose that the result must have a physical meaning applicable to stars, one is led to require that a number of constraints be satisfied. They can be summarized as follows:

1. The density must drop with the radius as a power law ($\rho(r) \propto r^k$) with an exponent k that is negative and has a modulus larger than unity.
2. The pressure must follow a similar trend, but with a slightly larger negative exponent, so that a polytropic relation of the type $P(r) \propto \rho(r)^\delta$ with $\delta \lesssim 4/3$ holds.
3. The *magnetic Prandtl number* P_m (namely, the ratio between the *kinematic* viscosity $\eta = \mu_d/\rho$, where μ_d is the *dynamic* viscosity, and the magnetic diffusivity ν_m) is much larger than unity (see Spitzer 1962).
4. While the *kinematic* viscosity η cannot be neglected, the *dynamic* viscosity μ_d remains low due to the low density (at the level of one to a few percent).

Once those conditions are verified, the radial velocity of magnetized structures turns out to be

$$v_r = \Gamma r^{-(k+1)}, \tag{5}$$

where $\Gamma = v_p r_p^{k+1}$. The parameters v_p and r_p refer to the buoyancy velocity and radial position of the innermost layer where the abovementioned conditions start to be satisfied, while k is the exponent in the relation $\rho \propto r^k$.

Below a convective envelope k is always rather large in absolute value but negative ($k \leqslant -3$); then Equation (6) yields an unstable condition, in which buoyancy starts slowly but then gains speed rapidly with an increasing radius. The toroidal component of the magnetic field can be correspondingly written as

$$B_\varphi = \Phi(\xi)\left(\frac{r_p}{r}\right)^{k+1}, \tag{6}$$

where ξ is an adimensional variable and $\Phi(\xi)$ can be chosen freely; for a simple solution it might even be a constant ($\Phi(\xi) = B_{\varphi,p}$). Again, we use a subscript p to indicate the values of parameters pertaining to the layer from which buoyancy (on average) starts. For more details on the solution and its stellar applications see Nucci & Busso (2014), Trippella et al. (2016), and Palmerini et al. (2017, 2018).

During the occurrence of a TDU episode, while the H-burning shell is extinguished, the above procedure describes a mass upflow that forces a downflow of protons from the envelope for mass conservation. In light of the above considerations, the mixing rate forced by magnetic buoyancy is

$$\dot{M} = 4\pi\rho_e r_e^2 v_e f. \tag{7}$$

Here v_e is the velocity of buoyant flux tubes at the envelope bottom, and the filling factor f is of the order of 10^{-5} (Trippella et al. 2016). By applying this equation to AGB stars of masses up to $5\,M_\odot$, we can obtain $\dot{M}$ values in the range of 10^{-7} to $10^{-5}\,M_\odot\,\mathrm{yr}^{-1}$.

The downflow of matter from the envelope, pushed down by the rising material, was analyzed in detail by Trippella et al. (2016) for the formation of a ^{13}C pocket and the subsequent neutron release via the ^{13}C$(\alpha, n)^{16}$O reaction. The ^{13}C reservoir varies in mass (by up to a factor of 3) during the sequence of TPs of an individual star. It varies more substantially as a function of the stellar mass.

A typical set of abundance profiles for protons and subsequently for ^{13}C and ^{14}N, as obtained with our model in the He-rich layers, is presented in Figure 2. Table 3 shows the extension in mass of the pocket at the sixth TDU episode of

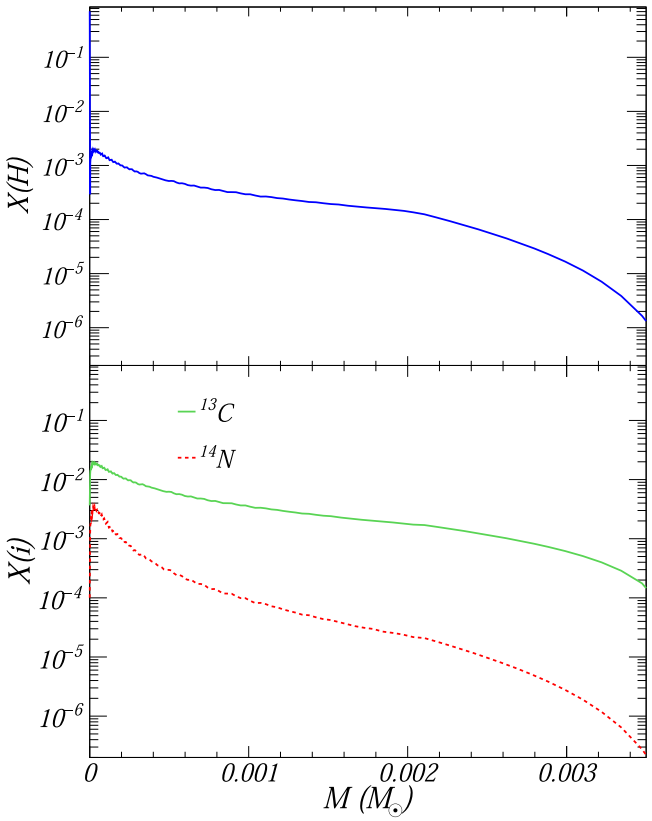

Figure 2. Upper panel: the proton profile established in the He-rich layers as a consequence of mass conservation, when magnetic buoyancy is occurring at a TDU episode. The case represented is a 3 $M_\odot$ star of solar metallicity at the sixth TDU. The extension is about 60% of what was found by Trippella et al. (2016) for a 1.5 $M_\odot$ model. Lower panel: the ensuing profiles of ^{13}C and ^{14}N formed after the H-shell reignition.

Table 3
Mass of the ^{13}C Pocket for Different Models

AGB Model	$\mu_d = 0.01$	$\mu_d = 0.05$
1.5 $M_\odot$, [Fe/H] = 0.0	$2.8 \cdot 10^{-3}\,M_\odot$	$4.9 \cdot 10^{-3}\,M_\odot$
2.0 $M_\odot$, [Fe/H] = 0.0	$2.6 \cdot 10^{-3}\,M_\odot$	$4.4 \cdot 10^{-3}\,M_\odot$
3.0 $M_\odot$, [Fe/H] = −0.5	$5.4 \cdot 10^{-4}\,M_\odot$	$1.4 \cdot 10^{-3}\,M_\odot$
5.0 $M_\odot$, [Fe/H] = 0.0	$1.5 \cdot 10^{-5}\,M_\odot$	$0.9 \cdot 10^{-4}\,M_\odot$

Table 4
SLRs as Predicted by a 3 $M_\odot$ Model with MHD Mixing

[Fe/H] = 0—Dilution $d = 9.05 \cdot 10^{-3}$—Delay Time $\Delta = 0.87$ Myr						
Rad.	Ref.	τ_R (Myr)	N^R/N^S	q^S	$\alpha^{R,S}$	$[N^R/N^S]_{\rm Meas.}$
^{26}Al	^{27}Al	1.03	$1.34 \cdot 10^{-2}$	1.004	$5.23 \cdot 10^{-5}$	$(5.23 \pm 0.13) \cdot 10^{-5}$
^{41}Ca	^{40}Ca	0.15	$1.48 \cdot 10^{-4}$	0.994	$4.00 \cdot 10^{-9}$	$4 \cdot 10^{-9}$
^{60}Fe	^{56}Fe	3.75	$2.18 \cdot 10^{-5}$	0.994	$1.55 \cdot 10^{-7}$	10^{-8}–10^{-6}
^{107}Pd	^{108}Pd	9.4	$1.33 \cdot 10^{-1}$	6.198	$6.78 \cdot 10^{-3}$	$(5.9 \pm 2.2) \cdot 10^{-5}$
^{135}Cs	^{133}Cs	3.3	$6.77 \cdot 10^{-1}$	2.101	$5.53 \cdot 10^{-3}$	$4.8 \cdot 10^{-4}$
^{182}Hf	^{180}Hf	12.8	$1.18 \cdot 10^{-2}$	4.027	$4.01 \cdot 10^{-4}$	$(9.81 \pm 0.41) \cdot 10^{-5}$
^{205}Pb	^{204}Pb	22	$6.58 \cdot 10^{-1}$	2.552	$1.46 \cdot 10^{-2}$	10^{-3}

Table 5
SLRs as Predicted by a 5 $M_\odot$ Model with MHD Mixing

[Fe/H] = 0—Dilution $d = 3.27 \cdot 10^{-2}$—Delay Time $\Delta = 0.85$ Myr						
Rad.	Ref.	τ_R (Myr)	N^R/N^S	q^S	$\alpha^{R,S}$	$[N^R/N^S]_{\rm Meas.}$
^{26}Al	^{27}Al	1.03	$3.65 \cdot 10^{-3}$	1.002	$5.23 \cdot 10^{-5}$	$(5.23 \pm 0.13) \cdot 10^{-5}$
^{41}Ca	^{40}Ca	0.15	$3.57 \cdot 10^{-5}$	0.996	$4.00 \cdot 10^{-9}$	$4 \cdot 10^{-9}$
^{60}Fe	^{56}Fe	3.75	$4.36 \cdot 10^{-4}$	0.995	$1.13 \cdot 10^{-5}$	10^{-8}–10^{-6}
^{107}Pd	^{108}Pd	9.4	$2.24 \cdot 10^{-2}$	1.139	$7.61 \cdot 10^{-4}$	$(5.9 \pm 2.2) \cdot 10^{-5}$
^{135}Cs	^{133}Cs	3.3	$3.09 \cdot 10^{-2}$	1.011	$7.60 \cdot 10^{-4}$	$4.8 \cdot 10^{-4}$
^{182}Hf	^{180}Hf	12.8	$3.66 \cdot 10^{-4}$	1.026	$1.15 \cdot 10^{-5}$	$(9.81 \pm 0.41) \cdot 10^{-5}$
^{205}Pb	^{204}Pb	22	$4.42 \cdot 10^{-2}$	1.038	$1.44 \cdot 10^{-3}$	10^{-3}

different stellar models (the metallicity is indicated in the common logarithmic spectroscopic notation [Fe/H] relative to the solar abundance, so that [Fe/H] = 0 means a solar metallicity and [Fe/H] = −0.5 means one-third solar). As is shown by the table, the size of the pocket is rather constant for low masses ($M \leqslant 2\,M_\odot$), while it rapidly drops to very small values for higher-mass AGB stars. The extensions of the *p*-enriched reservoir are shown for two choices of the starting layer for buoyancy: (i) one characterized by a dynamic viscosity of $\mu_d = 0.01$ and (ii) one where $\mu_d = 0.05$. This second value seems so far to be the one giving a more coherent interpretation of solar abundances (Trippella et al. 2016) and of isotopic anomalies in presolar grains (Palmerini et al. 2018). We shall therefore adopt it as a reference here.

The same basic mechanism drives DM in the H-rich layers below the convective envelope during H-shell burning. This mixes with the envelope (with the same process) products of proton captures, including the nucleus ^{26}Al, whose prediction is needed for our SLR calculations. Details on the determination of ^{26}Al abundance in the envelope have already been published and can be found in Palmerini et al. (2017).

On the basis of the above procedures, we have computed the envelope abundances of ^{26}Al and neutron-rich nuclei for several models; we shall discuss the results for a couple of typical cases among those indicated in Table 2.

One can apply the formula of Equation (5) to a couple of nuclei produced by a model star, thus fixing the two parameters *d* and Δ. Then one has to verify what kind of prediction this implies for the other radioactive nuclei in pristine solids.

For the reference nuclei we use ^{26}Al and ^{41}Ca. The motivation for this choice lies in the fact that it has been ascertained (Duprat & Tatischeff 2007; Villeneuve et al. 2009) that ^{26}Al cannot be produced by solar spallation and needs to derive from a stellar source. Moreover, the correlation between ^{26}Al and ^{41}Ca established by Sahijpal et al. (1998) and reported here in Figure 1 suggests that the two nuclei may have the same origin. We underline that this constraint is not considered in several published scenarios among those quoted, which appears to be a serious drawback: in fact, the mentioned correlation and the stellar origin for ^{26}Al represent important pieces of evidence and should be taken into account.

Tables 4 and 5 show the outcomes obtained by deriving the two free parameters from the mentioned nuclei (i.e., fixing *d* and Δ so that the measurements for ^{26}Al and ^{41}Ca in ESS solids are reproduced), adopting two typical models for IMSs from our calculations. They refer to a 3 $M_\odot$ and a 5 $M_\odot$ star, both with solar metallicity. (We do not discuss here in detail results for significantly lower masses, because of their excessively long lifetimes, essentially inhibiting any chance encounter with the forming Sun.)

The main result that can be derived from even a quick glance at Tables 4 and 5 is that when a ^{13}C pocket is included (even of minimal extension, as in the case of the 5 $M_\odot$ model), accounting for the lighter radioactive isotopes ^{26}Al and ^{41}Ca always implies some large excesses on nuclei heavier than iron. This is a very big problem: a deficit in isotopes like ^{107}Pd, ^{135}Cs, and ^{182}Hf, which are not purely of *s*-process origin, might be compensated by some inheritance of *r*-process products from Galactic evolution; but large excesses, like those shown in the tables, cannot be accommodated.

As mentioned, the main difference between our models and those by Wasserburg et al. (2006), where a nice solution could be found for several SLRs, is the presence of a ^{13}C pocket, which was instead excluded in that solution. Whatever the extension of the pocket is, the neutron flux remains always too large to find any consistency with ^{26}Al production. In light of our MHD model for the formation of the neutron source ^{13}C, we have no way to solve this inconsistency and must admit that a solution for SLRs in the framework of our models for mixing and nucleosynthesis in AGB stars can no longer be found.

5.2. Effects of a Late-AGB Star. II. Models with Opacity-induced Mixing

During a TDU, more than one physical mechanism can contribute to the downward diffusion of protons into the underlying He- and C-rich layer. Spectroscopic observations and presolar SiC grain measurements provide indications of the shape and extension of the ^{13}C pocket. Recent studies point to a flat ^{13}C profile in a region one to a few $10^{-3}\,M_{\odot}$ thick (see, e.g., Liu et al. 2014, 2015; Palmerini et al. 2018); in this respect both DM models considered in this work fulfill the basic requirements. Among the constraints, there is also a need to limit the abundance by mass of ^{13}C in each layer; otherwise a too large production of ^{14}N (a neutron poison) would be obtained, hampering *s*-processing. In the so-called "FRUITY" models (Cristallo et al. 2011, 2015b, 2016), the approach first discussed by Becker & Iben (1979) was followed. It considers the effects on mixing of the opacity difference between the (opaque) H-rich envelope and the (more transparent) He-rich underlying region. During a TDU, such a difference produces a discontinuity in the temperature gradient at the inner border of the envelope, which leads to a consequent abrupt decrease of the convective velocities (see Straniero et al. 2006). This process is unbalanced and unstable: any perturbation of the convective/radiative interface tending to expand downward the boundary would grow, thus leading to an even deeper mixing. In such a condition, it is reasonable to hypothesize that the result is not an extension of the envelope as a whole, but rather that individual convective elements with nonzero velocities penetrate beyond the limit defined by the Schwarzschild criterion (where the radiative gradient equals the adiabatic one). Those bubbles are decelerated by the steep pressure gradient immediately below the inner envelope border, which strongly limits the extent of their penetration. In order to mimic this behavior, we impose that bubble velocities below the formal Schwarzschild border decline exponentially—namely,

$$v = v_{\rm IN} \exp\left(-\frac{\Delta r}{\beta H_p}\right). \quad (8)$$

Here Δr is the distance from the Schwarzschild border, $v_{\rm IN}$ is the velocity of the most internal convective mesh, H_p is the pressure scale height at the border itself, and β is a free parameter (usually set to $\beta = 0.1$ on observational grounds; for its calibration see Cristallo et al. 2009). The introduction of this algorithm implies that

1. the convective border becomes more stable;
2. the TDU efficiency is increased; and
3. a profile of protons is left below the convective envelope.

As with the MHD instabilities discussed in the previous subsection, in this approach the mass extension of the pocket does not remain constant along the AGB but decreases steadily, following the shrinking of the He-intershell region with increasing core mass (Cristallo et al. 2009). A potential problem arising from this approach is that the exponential decline of convective velocities would proceed to the center of the star, unless a maximum penetration is fixed. This limit was initially set to $2H_p$ (Straniero et al. 2006). Later, a better match to isotopic ratios in presolar SiC grains (Liu et al. 2014, 2015) suggested fixing the penetration limit in terms of the convective velocity, imposing that it stops at a certain small fraction

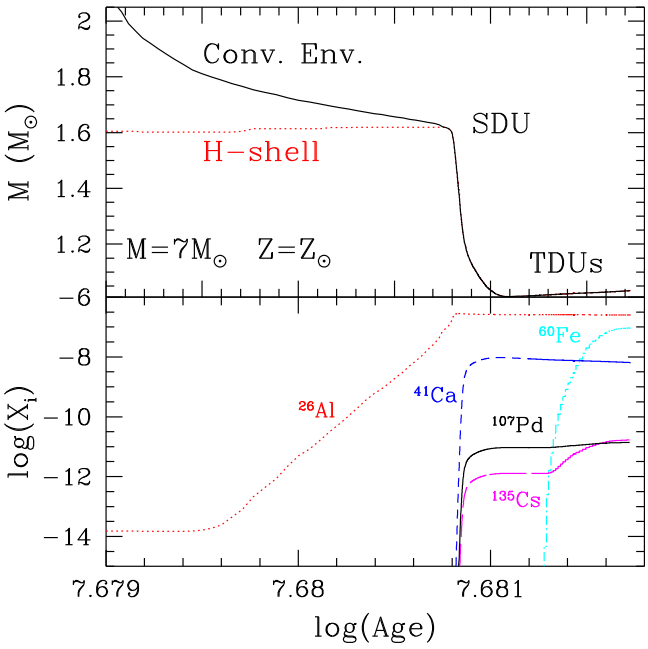

Figure 3. Upper panel: temporal evolution of the mass coordinates of the H-burning shell and of the inner border of the convective envelope for a 7 $M_{\odot}$ model with solar metallicity. Lower panel: temporal evolution of surface abundances for some radioactive isotopes of interest.

(10^{-11}) of the value achieved at the Schwarzschild border. This corresponds to a depth of 2.2–2.3H_p.

The ^{13}C pockets obtained with the method outlined above are not remarkably different from those proposed by Trippella et al. (2016) and discussed in Section 5.1, although they are characterized by a larger amount of ^{14}N in the upper region. This feature is intrinsically connected to the approach followed, which yields a top-down flow of the material (and not a bottom-up movement, like that of magnetic tubes characterizing the models of Section 5.1).

We refer the reader to Cristallo et al. (2015a, 2016) and references therein for a detailed description of the nucleosynthesis resulting from the assumptions outlined above. Here we recall simply that the models discussed are rather "cool" (e.g., cooler than those outlined in Section 5.1) and because of this do not experience HBB, a process that, as already mentioned, has a strong model dependency.

For the specific purposes of this work and in the framework of the approach just discussed, we integrate the FRUITY database by also computing more massive AGB models ($6.5 \leqslant M/M_{\odot} \leqslant 8$) at solar metallicity. The surface isotopic distributions of those masses include the effects of the SDU. This event has a considerable impact on radioactive isotope abundances. As already highlighted, SDU occurs during the early-AGB phase of IMSs; in that phase, the switching off of the H-burning shell is followed by the inward penetration of the convective envelope in the H-depleted zone (upper panel of Figure 3). As widely reported in the literature, among the consequences of the SDU there is an increase of the surface ^{4}He, ^{14}N, and ^{26}Al abundances. A further effect present in our models induces enhancements for at least three more SLRs of interest beyond ^{26}Al: they are ^{41}Ca, ^{107}Pd, and ^{135}Cs, ensuing from a marginal neutron capture episode (see the lower panel of Figure 3, which also shows ^{60}Fe). Indeed, those isotopes are produced by the radiative burning of the amount of ^{13}C present in H-burning ashes (its CNO equilibrium abundance). This

Table 6
SLRs as Predicted by a 6 $M_{\odot}$ Model

[Fe/H] = 0—Dilution $d = 5.18 \cdot 10^{-2}$—Delay Time $\Delta = 0.98$ Myr						
Rad.	Ref.	τ_R (Myr)	N^R/N^S	q^S	$\alpha^{R,S}$	$[N^R/N^S]_{\rm Meas.}$
^{26}Al	^{27}Al	1.03	$2.64 \cdot 10^{-3}$	0.991	$5.23 \cdot 10^{-5}$	$(5.23 \pm 0.13) \cdot 10^{-5}$
^{41}Ca	^{40}Ca	0.15	$5.42 \cdot 10^{-5}$	0.980	$4.00 \cdot 10^{-9}$	$4 \cdot 10^{-9}$
^{60}Fe	^{56}Fe	3.75	$1.32 \cdot 10^{-5}$	1.008	$5.30 \cdot 10^{-7}$	10^{-8}–10^{-6}
^{107}Pd	^{108}Pd	9.4	$2.31 \cdot 10^{-2}$	1.200	$1.29 \cdot 10^{-3}$	$(5.9 \pm 2.2) \cdot 10^{-5}$
^{135}Cs	^{133}Cs	3.3	$3.75 \cdot 10^{-2}$	1.007	$1.39 \cdot 10^{-3}$	$4.8 \cdot 10^{-4}$
^{182}Hf	^{180}Hf	12.8	$1.21 \cdot 10^{-2}$	1.271	$7.34 \cdot 10^{-4}$	$(9.81 \pm 0.41) \cdot 10^{-5}$
^{205}Pb	^{204}Pb	22	$1.73 \cdot 10^{-2}$	1.099	$9.39 \cdot 10^{-4}$	10^{-3}

Table 7
SLRs as Predicted by a 7 $M_{\odot}$ Model

[Fe/H] = 0—Dilution $d = 3.32 \cdot 10^{-2}$—Delay Time $\Delta = 1.01$ Myr						
Rad.	Ref.	τ_R (Myr)	N^R/N^S	q^S	$\alpha^{R,S}$	$[N^R/N^S]_{\rm Meas.}$
^{26}Al	^{27}Al	1.03	$4.31 \cdot 10^{-3}$	0.976	$5.23 \cdot 10^{-5}$	$(5.23 \pm 0.13) \cdot 10^{-5}$
^{41}Ca	^{40}Ca	0.15	$1.05 \cdot 10^{-4}$	0.980	$4.00 \cdot 10^{-9}$	$4 \cdot 10^{-9}$
^{60}Fe	^{56}Fe	3.75	$6.79 \cdot 10^{-5}$	1.008	$1.74 \cdot 10^{-6}$	10^{-8}–10^{-6}
^{107}Pd	^{108}Pd	9.4	$1.21 \cdot 10^{-2}$	1.078	$3.88 \cdot 10^{-4}$	$(5.9 \pm 2.2) \cdot 10^{-5}$
^{135}Cs	^{133}Cs	3.3	$1.24 \cdot 10^{-2}$	0.963	$2.79 \cdot 10^{-4}$	$4.8 \cdot 10^{-4}$
^{182}Hf	^{180}Hf	12.8	$7.24 \cdot 10^{-3}$	1.132	$2.51 \cdot 10^{-4}$	$(9.81 \pm 0.41) \cdot 10^{-5}$
^{205}Pb	^{204}Pb	22	$1.03 \cdot 10^{-2}$	0.992	$3.23 \cdot 10^{-4}$	10^{-3}

occurs because the layers beyond the H-burning shell are heated up to more than 10^8 K, i.e., to high enough temperatures to activate the ^{13}C$(\alpha, n)^{16}$O reaction. Later, surface abundances are further changed by TDUs (although not for all isotopes). Note that a similar finding has never been reported in the literature, because post-process calculations commonly ignore the nucleosynthesis of heavy elements before the TP-AGB phase. Our FRUITY stellar evolutionary models are instead computed with a full nuclear network, starting from the main sequence phase and extending up to the tip of the AGB.

Once all the above effects are considered, the final surface abundances of radioactive nuclei in our models can be used to estimate their possible contribution to their inventory in the ESS. Tables 6 and 7 summarize these results for two typical cases. Much like what we obtain in Section 5.1, in this case there is also no space for a compromise agreement. The predictions always include excesses of some heavy ($A > 56$) neutron capture nuclei (especially ^{107}Pd) with respect to ^{26}Al and ^{41}Ca (from which, again, we deduce the time delay Δ and the dilution factor d). We argue that this conclusion is not limited to the specific models considered in this work as examples: any DM model yielding proton penetration into the He-rich layers, inducing the formation of a ^{13}C pocket, will inevitably end up with excesses of ^{107}Pd and other neutron-rich isotopes with respect to the lighter ones.

Figure 4 summarizes the results of this section, showing the predictions from both Sections 4.1 and 4.2; they can be represented together thanks to the similarity of the findings, despite the different (complementary) starting hypotheses. Over the mass range of about 2 to about 8 $M_{\odot}$, when one constrains the free parameters Δ and d through a fit of the measured ESS abundances of ^{26}Al and ^{41}Ca, heavier nuclei are not simultaneously accounted for, and in all cases the most relevant problem resides in the huge overproduction of ^{107}Pd. This fact leads us to the conclusion that the scenario of solar system pollution by an AGB star of intermediate mass may be inadequate, although for the most massive models a window is still open. In particular, our models are rather cool and do not develop HBB. As mentioned, this process has been examined by Wasserburg et al. (2017), with negative conclusions. However, HBB is still strongly model-dependent. One would need an ad hoc H-burning process at the base of the envelope to produce ^{26}Al in exactly the right amount to compensate for the excesses in n-rich isotopes induced by the presence of a ^{13}C pocket. The reality of this possibility, however, must be explored in detail. This will be the subject of a forthcoming work.

6. Nucleosynthesis in MSs and the Role of Late SNe

MSs are defined as stars that can contract and heat up to several billions of degrees, eventually reaching the conditions for collapse of the core up to nuclear densities. Depending on the initial metallicity, the initial rotational velocity, and the treatment of the convective borders, the minimum mass suitable to evolve up to the final stages ranges somewhere between 9 and 12 $M_{\odot}$. This limit also marks the maximum mass of so-called super-AGB stars, i.e., those that form a strongly electron-degenerate core only after burning C and/or Ne. The evolution of these stars is characterized by weak but very frequently repeated TPs and may end with the formation of O–Ne white dwarfs or electron capture SNe (Denissenkov et al. 2013; Doherty et al. 2017). The possible contributions of super-AGB stars to the inventory of ESS radioactivities were first analyzed by Lugaro et al. (2012); they will not be rediscussed here, in view of the large uncertainties and model dependencies related to the very complex physics still affecting this mass range.

Since MSs avoid electron degeneracy and evolve toward higher and higher temperatures, they activate nuclear reactions that form increasingly heavier nuclei through the H-, He-, C-, Ne-, O-, and Si-burning phases. Once the temperature reaches $\sim$10 GK, electrons become relativistic, and the contraction

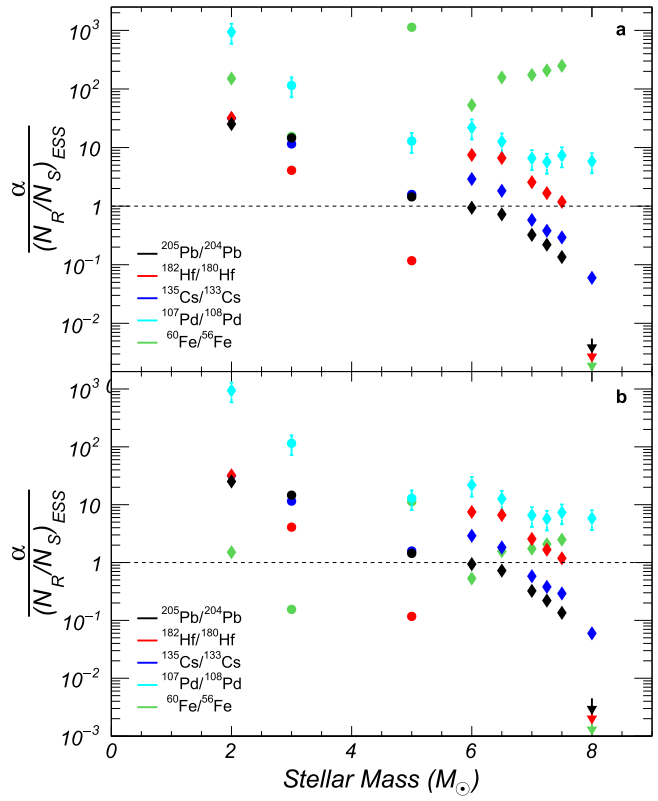

Figure 4. Prediction for heavy SLRs from AGB stars with the physical models for DM discussed in Sections 4.1 and 4.2. In panel (a) we adopt as a reference ESS ratio for ^{60}Fe/^{56}Fe the value of 10^{-8}, while in panel (b) the opposite extreme choice is made (10^{-6}). The figure shows that when the free parameters Δ and d are fixed through a fit of the measured ESS abundances of ^{26}Al and ^{41}Ca, heavier nuclei are not satisfactorily accounted for. As an example, even the models explaining ^{60}Fe well (those around 6–7 $M_\odot$, in panel b) always imply excesses by a factor of 8–20 on ^{107}Pd. (In the plot, dots indicate the models of Section 5.1, and diamonds those of Section 5.2. The case of 2 $M_\odot$ illustrated here is not explicitly specified in a table, due to its too long lifetime that would make a chance encounter with the forming Sun impossible. It is shown here only to illustrate the rather smooth and continuous sequence of behaviors characterizing the two series of models that, although different, converge to a rather unique and coherent view of AGB phases.)

reverses into a collapse of the core. Here nuclear densities are reached, eventually driving the phenomenon of CCSN explosion. The ensuing shock wave causes the violent expulsion of the external layers into the ISM. The very high peak temperature achieved by the innermost layers as the shock front moves outward induces a substantial modification of the pre-existing composition; this means that it is not correct to neglect the nucleosynthesis induced by the passage of the shock wave (explosive nucleosynthesis) if one wants to study the contribution of MSs to Galactic enrichment and to the ESS composition. Unfortunately, some of the works present in the literature on ESS radioactivities do not take explosive phases into account. This is particularly the case for some scenarios for the sequential contamination of a presolar molecular cloud (Gounelle et al. 2006; Gounelle & Meynet 2012). One should therefore look at these results with a bit of caution.

In the external layers of the star, through which the shock wave passes, relics of core He-burning and shell C-burning are abundant. These zones include *s*-process isotopes, having experienced *n*-captures, mainly from the ^{22}Ne(α, n)^{25}Mg source, during the quiet evolution of the SN progenitor. They are actually considered the main site where the *weak s*-process component is generated (Raiteri et al. 1993; Pignatari et al. 2010), producing isotopes up to those of Sr, sited at the "magic" neutron number $N = 50$. Above this mass region, neutron captures in MSs become rather inefficient, but they might still play a role in the ESS radioactivities, as these were typically produced in environments with small enhancement factors q^s (see also Section 5).

In the scenario of solar system formation, an MS forming a CCSN has been suggested by several authors as a potential trigger for inducing the final collapse of the presolar cloud through shock waves (Cameron & Truran 1977; Vanhala & Boss 2002; Boss 2003). This event must have been accompanied by a strong injection of newly formed nuclei into the ESS, including SLRs like ^{26}Al, ^{41}Ca, ^{60}Fe, and ^{53}Mn, plus possibly those synthesized in fast and slow *n*-capture processes. Also many stable isotopes of major elements are expected to receive important contributions. Hence, by modeling the processes of hydrostatic and explosive nucleosynthesis in massive pre-SN and during the final CCSN events, one can predict the isotopic anomalies that such a pollution would have induced in the solar nebula.

As already mentioned, CCSNe are typically the main producers of intermediate-mass elements, from O to Ti; they also synthesize C, iron-peak nuclei, and the weak component of the *s*-process. In order to evaluate the possibility that a late SN event was responsible for polluting the ESS with radioactive species not accounted for by the average Galactic enrichment (Section 3), it is also necessary to estimate the total variations that this would imply both in the solar abundances of stable elements and in their isotopic admixture. These contributions strongly depend on the initial stellar mass, on the chemical composition, and on the rotational properties of the stellar models.

In this work we consider as possible contaminating candidates stars that are parents to CCSNe, having a solar metallicity and an initial mass in the range of 13 to 25 $M_\odot$. The models are computed with the FRANEC evolutionary code (Chieffi & Limongi 2013, 2015) and include the effects of rotation. The main consequence of including rotation is that of increasing the total yields of the elements, because it basically produces additional mixing processes, thus more efficiently feeding the burning layers with fresh fuels. For our purposes, we consider a set of models with masses of 13, 15, 20, and 25 $M_\odot$ and initial equatorial rotational velocities of 0, 150, and 300 km s^{-1}. Each model is evolved from the pre–main sequence up to the onset of the core bounce with the FRANEC code. The explosive phases are then computed by reprocessing the structure and composition left after the hydrostatic phases through a hydrodynamical code, which takes into account the passage of the shock wave and the occurrence of explosive nucleosynthesis. The explosion is simulated in each case by considering the mixing and fallback mechanism (Umeda & Nomoto 2002). Within the mixing and fallback scenario, it is assumed that after the passage of the shock wave, a fraction of the most internal zone of the star is homogeneously mixed before fallback on the remnant of part of the ejected material occurs. In these models the inner border of the mixed region is set at the layer where [Ni/Fe] = 0.2, while the outer border is fixed at the base of the O shell (X(O) = 0.001). Then, the mass cut between ejected and non-ejected material is chosen by requiring that 0.07 $M_\odot$ of ^{56}Ni be ejected, thus reproducing the known iron production from SN 1987A (Li et al. 1993).

Table 8
SLRs as Predicted by a Nonrotating 20 $M_\odot$ Model

[Fe/H] = 0—Dilution $d = 1.85 \cdot 10^{-4}$—Delay Time $\Delta = 1.34$ Myr						
Rad.	Ref.	τ_R (Myr)	N^R/N^S	q^S	$\alpha^{R,S}$	$(N^R/N^S)_{\rm Meas.}$
^{26}Al	^{27}Al	1.03	$5.42 \cdot 10^{-3}$	192.2	$5.23 \cdot 10^{-5}$	$(5.23 \pm 0.13) \cdot 10^{-5}$
^{41}Ca	^{40}Ca	0.15	$1.68 \cdot 10^{-3}$	99.52	$4.00 \cdot 10^{-9}$	$4 \cdot 10^{-9}$
^{53}Mn	^{55}Mn	5.3	$5.75 \cdot 10^{-1}$	13.88	$1.15 \cdot 10^{-3}$	$(6.7 \pm 0.56) \cdot 10^{-6}$
^{60}Fe	^{56}Fe	3.75	$3.44 \cdot 10^{-4}$	16.80	$7.48 \cdot 10^{-7}$	10^{-8}–10^{-6}
^{135}Cs	^{133}Cs	3.3	$4.13 \cdot 10^{-2}$	14.43	$6.95 \cdot 10^{-5}$	$4.8 \cdot 10^{-4}$
^{205}Pb	^{204}Pb	22	$1.54 \cdot 10^{-1}$	12.19	$3.27 \cdot 10^{-4}$	10^{-3}

Table 9
SLRs as Predicted by a 25 $M_\odot$ Model with Rotational Velocity of 150 km s^{-1}

[Fe/H] = 0—Dilution $d = 9.11 \cdot 10^{-5}$—Delay Time $\Delta = 1.41$ Myr						
Rad.	Ref.	τ_R (Myr)	N^R/N^S	q^S	$\alpha^{R,S}$	$(N^R/N^S)_{\rm Meas.}$
^{26}Al	^{27}Al	1.03	$1.08 \cdot 10^{-2}$	209.5	$5.23 \cdot 10^{-5}$	$(5.23 \pm 0.13) \cdot 10^{-5}$
^{41}Ca	^{40}Ca	0.15	$3.01 \cdot 10^{-3}$	179.7	$4.00 \cdot 10^{-9}$	$4 \cdot 10^{-9}$
^{53}Mn	^{55}Mn	5.3	$5.44 \cdot 10^{-1}$	14.08	$5.35 \cdot 10^{-4}$	$(6.7 \pm 0.56) \cdot 10^{-6}$
^{60}Fe	^{56}Fe	3.75	$7.38 \cdot 10^{-4}$	17.80	$8.21 \cdot 10^{-7}$	10^{-8}–10^{-6}
^{135}Cs	^{133}Cs	3.3	$1.43 \cdot 10^{-1}$	18.10	$1.45 \cdot 10^{-4}$	$4.8 \cdot 10^{-4}$
^{205}Pb	^{204}Pb	22	$3.05 \cdot 10^{-1}$	21.63	$5.64 \cdot 10^{-4}$	10^{-3}

Tables 8 and 9 show how all the models considered do produce SLRs, especially ^{53}Mn and ^{60}Fe. In particular, again fixing the dilution factor d and the time delay Δ so that ^{26}Al and ^{41}Ca are reproduced, we see that the 25 $M_\odot$ model, in cases characterized by high rotation velocity and adopting the highest choices of the ^{60}Fe/^{56}Fe ratio in the ESS ($\simeq 10^{-6}$), would account rather well for ^{60}Fe itself and would imply the ratio ^{205}Pb/^{204}Pb within a factor of two from the measurement. It would however also yield some deficit in ^{135}Cs, which, as seen, cannot be compensated by contributions from the Galactic evolution of r-process nuclei (despite the fact that this isotope is not shielded against fast r-process decays). ^{53}Mn would be overabundant by almost two orders of magnitude and would require a special mass cut, as suggested by Meyer & Clayton (2000). (^{107}Pd and ^{182}Hf are not in the network adopted in the original models, and their abundances cannot be checked.)

These results are also reported in Figures 5 and 6 for the two extreme choices of the ^{60}Fe/^{56}Fe abundance in the ESS (10^{-8} for Figure 5 and 10^{-6} for Figure 6). As is shown, only in the second case, a 25 $M_\odot$ model with a high rotation rate ($\geqslant$150 km s^{-1}), does one obtain reasonable agreement between some of the measurements and predictions. However, ^{53}Mn remains largely overproduced (by two orders of magnitude). In any case, the scenario of Figure 6 requires a very large ^{60}Fe abundance in the ESS.

Furthermore, one notices that even fixing ad hoc the mass cut for accommodating ^{53}Mn, unsolved problems would remain for the abundances of stable isotopes. This is so to the point that we have serious doubts that any one of the cases studied can be reconciled with the measurements. This includes the models mentioned above, fitting most of the SLRs except for ^{53}Mn. We note that the exercise of adding these ejecta to the forming star in a very simple way, with complete and homogeneous mixing of the two components, would simply shift the abundances of stable nuclei without producing isotopic heterogeneities. However, more realistic scenarios that consider the possible clumpiness of ejecta or mass segregation imply the introduction of shifts in stable isotope abundances at levels incompatible with the limits set by actual measurements, as discussed previously. As an example, let us assume that these shifts are of the same order of magnitude of the average variations introduced in stable elements in the mentioned simple exercise. These shifts are shown in Figure 7 for the isotopes ^{16}O, ^{24}Mg, ^{28}Si, and ^{40}Ca in terms of per mill (delta) values. As shown in the plots, the anomalies predicted are at least a few percent. These are much larger than allowed by present uncertainties in meteoritic data, as discussed in Section 2. The fact that the injection process is complex and involves either the formation of clumpy structures or the incorporation of only part of the material ejected has been addressed by various authors (Goswami & Vanhala 2000; Maeda et al. 2008; Pan et al. 2012) and seems to be required by the same inhomogeneities of observed SN remnants. Clearly, hydrodynamical models of these mixing processes should consider all the SLRs, to complement the cases recently studied by Dwarkadas et al. (2018) for ^{26}Al and ^{60}Fe.

In view of these complexities and of the fact that huge shifts are found in Figure 7 for elements produced in vastly different layers of the star, very ad hoc hypotheses seem to be required by any mixing model aiming at eliminating them. We also recall that effects of the same order as found by us were present in the specific model of a 11.8 $M_\odot$ star by Banerjee et al. (2016). Those authors considered the excesses found on stable isotopes acceptable, but some of them are well in excess of 1%, so that they have the same problems encountered here.

A crucial and subtle problem concerning the anomalies in stable nuclei introduced by the mixing of freshly added material from an exotic source was underlined years ago by Nichols et al. (1999). Computing such stable shifts involves mixing model yields with measured abundances. Systematic errors in model yields can give unrealistic estimates of stable isotope anomalies. Nichols et al. (1999) tried to address this issue by mixing stellar ejecta into proxy compositions derived from chemical evolution calculations. These calculations used the same stellar yields adopted in the injected matter, to normalize out the errors. According to these calculations by

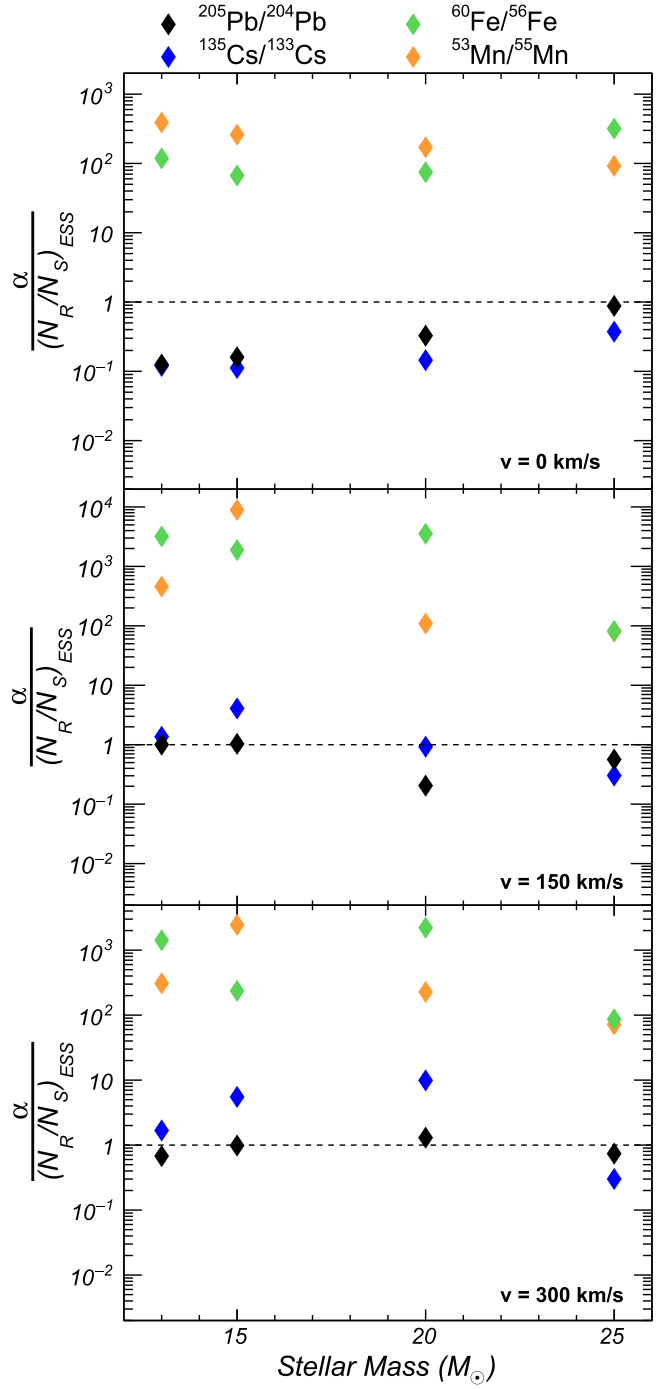

Figure 5. Predictions for SLRs from a late contamination by a CCSN in the mass range 13–25 $M_\odot$, assuming as a reference a solar ^{60}Fe/^{56}Fe ratio of $1 \cdot 10^{-8}$. Not one of the models shown can account acceptably for the measurements once ^{26}Al and ^{41}Ca are used for fixing the free parameters. In particular, ^{60}Fe and ^{53}Mn would be in any case enormously overproduced.

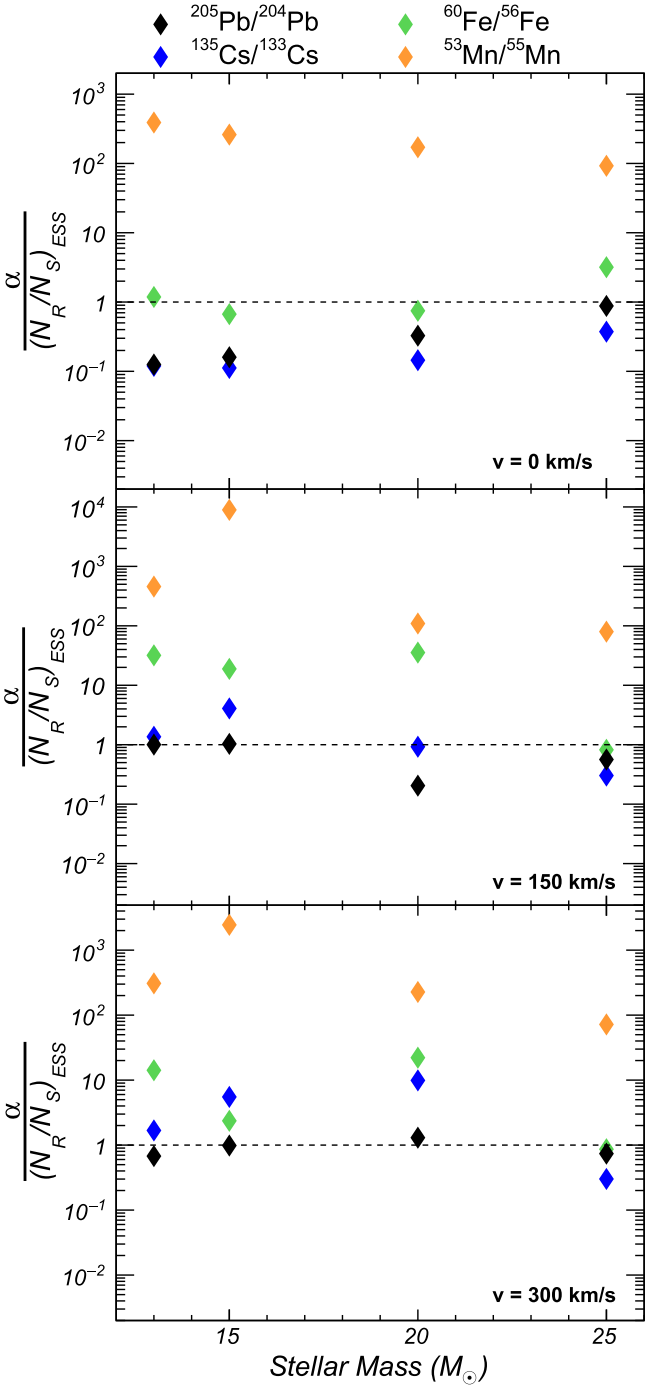

Figure 6. Predictions for SLRs from a late contamination by a CCSN in the mass range 13–25 $M_\odot$, assuming as a reference a solar ^{60}Fe/^{56}Fe ratio of $1 \cdot 10^{-6}$. As the figure shows, in this second case the models with no rotation up to 20 $M_\odot$ and the model of 25 $M_\odot$ with a rather high rotation rate ($\geqslant$150 km s^{-1}) would account reasonably for ^{60}Fe (in addition to ^{26}Al and ^{41}Ca, which are used for fixing the parameters), avoiding overproductions for ^{107}Pd and ^{135}Cs. However, ^{53}Mn would remain, also in this case overproduced by two orders of magnitude, and would require a much larger mass cut, as in Meyer & Clayton (2000).

Nichols et al. (1999), expected anomalies in stable isotope abundances are typically at the per mill level with only a few outliers at the percent level. Overall, the inferred anomalies are lower than those predicted here (see Figure 7) but are in many cases also incompatible with meteorite data (see Section 2).

7. Conclusions

In this paper we discuss a series of problems emerging in attempts at accounting for the presence of isotopic anomalies in early solids of the solar system, induced by the in situ decay of SLRs. Such problems become really difficult to handle if one wants to get a comprehensive scenario, indicating a series of Galactic processes capable of accounting for nuclides with lifetimes in the range of 10–20 Myr, like ^{107}Pd, ^{129}I, and ^{182}Hf, and for the shorter-lived isotopes ^{26}Al, ^{41}Ca, ^{53}Mn, ^{60}Fe, and

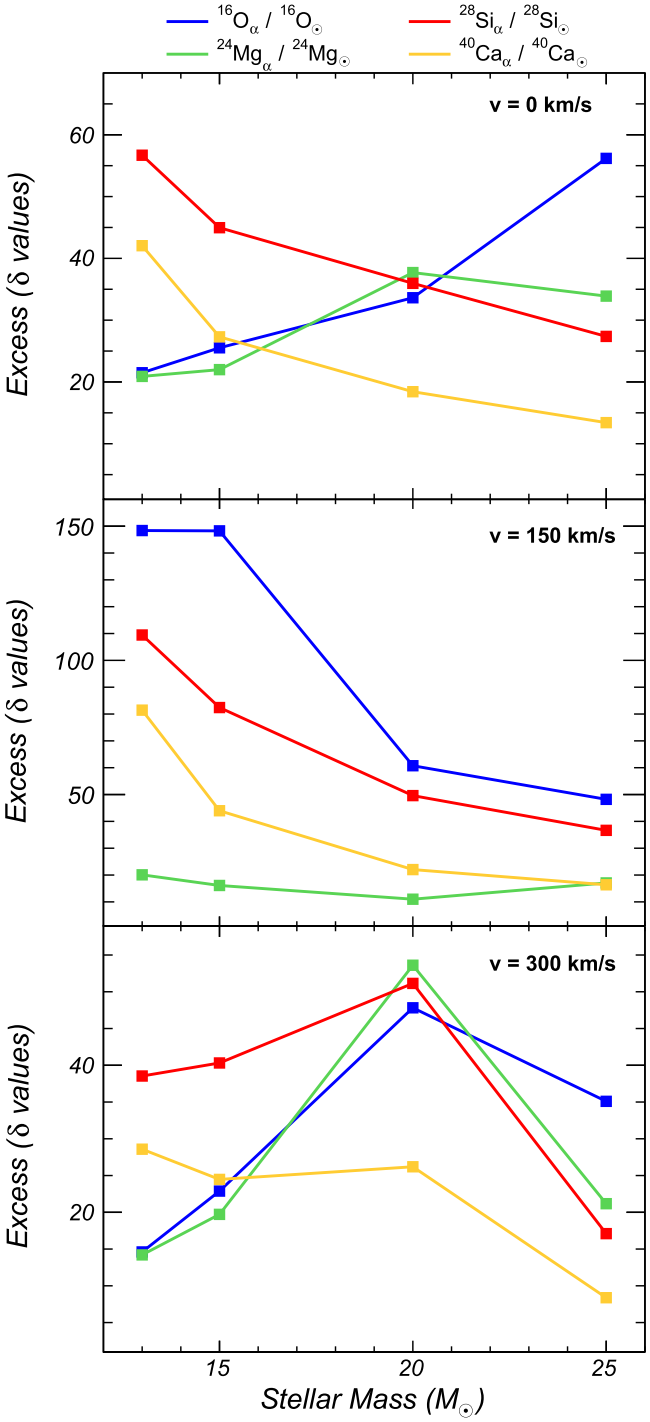

Figure 7. Values of the excesses introduced on α-rich isotopes of major stable elements by the CCSN models discussed so far, tuned to account for the $^{26}Al/^{27}Al$ and $^{41}Ca/^{40}Ca$ number ratios in the ESS. The plot shows the increase with respect to the accepted average abundances. We recall that shifts in excess of a few per mill are excluded by present-day measurements (see Section 2).

^{135}Cs. This leads us to conclude that a self-consistent understanding of the astrophysical origins for all the mentioned anomalies is still far from being obtained. In order to limit the uncertainties and update previous works on the subject, for the longer-lived nuclei we have tried to outline possible scenarios emerging from present-day lively debates on the astrophysical sources of the *r*-process, tentatively identifying in NSM nucleosynthesis—or in a complex, short-term granularity of the Galactic admixture of contributions from different sources—the origin of the low abundance of ^{129}I relative to the other neutron-rich nuclides. We consider the first hypothesis as the most probable today. For isotopes of lifetimes shorter than about 5 Myr we have instead pursued our analysis on the basis of very recent calculations of stellar evolution, from 2 to 25 $M_\odot$. For IMSs, this implies reference to current physical models for DM processes and to their implications for the activation of the neutron source $^{13}C(\alpha, n)^{16}O$. For MSs, the approach adopted includes up-to-date models with rotation, also accounting in detail for the final explosive phases. We believe that some of the frequently quoted discussions presented so far do not adequately consider the above issues; when this is done properly, several embarrassing open questions do remain.

In general, we have shown that the continuous nuclear evolution of the Galaxy over timescales of the order of 10 Gyr might account for the radioactivities measured in the early solar nebula having lifetimes τ_R longer than about 5 Myr, including ^{53}Mn. As mentioned, it is possible that the inclusion in this picture of peculiar NSM events, yielding high ratios between the abundances of nuclei at the third and second *r*-process peaks, also permits an explanation for the low abundance of ^{129}I. Shorter-lived isotopes, however, cannot be explained in this way. In particular, in addition to the known problematic cases of ^{26}Al, ^{41}Ca, and (possibly) ^{60}Fe, we have shown that ^{135}Cs also requires an ad hoc, late-minute contribution. There is therefore a necessity to assume a late addition of nucleosynthetic products for explaining the presence of very short-lived nuclei, including the exceptionally abundant ^{26}Al, which still poses the mentioned unanswered questions.

In the case of a late MS, two relevant problems exist, which go beyond its capability of accounting for this or that SLR in a suitable amount. The first is the apparently unavoidable introduction into the forming solar nebula of large anomalies in stable isotopes that are excluded by present measurements. The second difficulty, recognized for a long time, concerns the possibility that the fast winds of an SN explosion can really interact with a star-forming cloud without disrupting it and instead be homogeneously mixed with the cool material of the cloud itself. Also, from the point of view of the quantitative yields in SLRs, a late MS would need very special conditions to avoid introducing enormous excesses in ^{53}Mn, while it might fulfill the requirements imposed by ^{26}Al, ^{41}Ca, ^{135}Cs, and perhaps also ^{205}Pb.

The problem of mixing fast SN winds with cool condensing matter in a star-forming region might be avoided in the case, suggested recently, of a sequential pollution of the molecular cloud where the Sun was born, in which the last contribution might come from a dense shell formed at the external border of a WR wind, transporting cool matter and dust (Gounelle & Meynet 2012; Dwarkadas et al. 2017, 2018). One might guess that these models might or might not encounter the mentioned problems of excesses on stable isotopes, depending on the dilution factor and the degree of homogenization. However, some of the most quoted discussions in the literature do not consider the effects of previous SNe with an adequate and detailed computation of explosive nucleosynthesis; should this be done, we believe that the problems encountered here with a single-star pollution would remain. As a simple example, if the Sun was born in a giant molecular cloud similar to the ones we

know today (having masses of 10^5 to $3 \cdot 10^6\,M_\odot$; see, e.g., Solomon et al. 1979), then the mixing over the whole cloud of typically $20\,M_\odot$ of ejecta from a CCSN would yield a dilution factor in the range of $2 \cdot 10^{-4}$ (similar to that of Table 8) to $0.6 \cdot 10^{-5}$. In the first case, the process of homogenization of the ejecta would probably be incomplete, so that, as in Figure 7, excesses on stable nuclei at levels incompatible with measurements would remain; in the second, the excessive dilution would not explain any SLR except perhaps ^{60}Fe. Possible improvements in the above not encouraging views might come from considerations of asphericities in the SN ejecta, whose effects on the solar system formation are, however, at the moment only speculation (Dwarkadas et al. 2017). We stress again that any attempt at obtaining a compromise solution in this field should necessarily be based on quantitative models for explosive processes and for their nucleosynthesis.

Concerning less massive stars, which end their life cycle with the described TP-AGB phases, their models recently evolved from being fully parameterized to considering the physical mechanisms that can induce nonconvective mixing. These mechanisms also control the introduction of proton flows into the He-rich layers at the TDU. It is found that all stars, up to at least 7–8 $M_\odot$, would form a reservoir of ^{13}C. This is bound to induce neutron production through the ^{13}C$(\alpha,\ n)^{16}$O reaction, an occurrence that may prove fatal to the old scenario devised by Wasserburg et al. (1994, 2006) and Busso et al. (2003). Indeed, the neutron fluences ensuing from it, adding their effects on those from the ^{22}Ne$(\alpha, n)^{25}$Mg reaction, always yield large excesses of neutron capture radioactive isotopes, especially ^{107}Pd, with respect to ^{26}Al. In order to limit model dependencies, this fact is shown to occur with reference to two different treatments for DM mechanisms.

A limited parameter space remains to be explored, in the picture of a single late nucleosynthetic episode, for attempting to explain the shortest-lived radioactivities of the ESS (those with $\tau_R \lesssim 5$ Myr). One possibility resides in the already mentioned super-AGB stars, objects in a narrow mass interval (from about 9 to about 11 $M_\odot$, variable with the metallicity) between IMSs and MSs. Since the mass of the ^{13}C pocket steadily decreases with an increasing initial mass of the parent star, in that mass region it might go essentially to zero, thus avoiding the extra production of neutron-rich nuclei, which in the present work appears to hamper the possibilities previously envisioned by Wasserburg et al. (2006) and by Trigo-Rodríguez et al. (2009). An alternative might also be found in the most massive among IMSs (7–8 $M_\odot$) if HBB calculations, which are still largely model-dependent, are found to be less effective than discussed by Wasserburg et al. (2017), thus allowing one to obtain more limited ^{26}Al/^{107}Pd ratios.

Coming instead to schemes of the sequential contamination of a presolar molecular cloud, one should find a path in the fine-tuning of the many free parameters involved in those models, such that the CCSNe that occurred in early epochs of the molecular cloud's life do not introduce too large excesses on stable isotopes and nevertheless succeed in producing in adequate quantities the required SLRs not accounted for by a possible last (and non-exploding) WR event (e.g., ^{41}Ca, ^{53}Mn, ^{135}Cs, and possibly ^{205}Pb). One might also speculate that all SLRs except ^{26}Al, ^{41}Ca, ^{53}Mn, and ^{60}Fe might be produced in a burst of nucleosynthesis during an NSM event, which would avoid the excesses on stable isotopes related to CCSNe. Our knowledge of these elusive but important phenomena, however, is still in its infancy, and any further guess seems to be so far premature.

We all are indebted to a very competent referee willing to provide us with important advice on various aspects of the work in a very constructive and helpful way. D.V. is grateful to Gran Sasso Science Institute and to the INFN Section of Perugia for establishing the collaboration that permitted this work. M.B., S.P., and O.T. are also grateful to the Department of Physics and Geology of Perugia for its financial support. S.P. thanks Fondazione Cassa di Risparmio di Perugia for its three-year grant, under which this work was performed.

ORCID iDs

D. Vescovi https://orcid.org/0000-0003-0309-4666
O. Trippella https://orcid.org/0000-0002-4757-0487
S. Cristallo https://orcid.org/0000-0001-9683-9406
L. Piersanti https://orcid.org/0000-0002-8758-244X
M. Limongi https://orcid.org/0000-0003-0636-7834
P. Hoppe https://orcid.org/0000-0003-3681-050X

References

Abbott, B. P., Abbott, R., Abbott, T. D., et al. 2017, ApJL, 848, L12
Atanasov, D., Ascher, P., Blaum, K., et al. 2015, PhRvL, 115, 232501
Baker, R. G. A., Schönbächler, M., Rehkämper, M., Williams, H. M., & Halliday, A. N. 2010, E&PSL, 291, 39
Banerjee, P., Qian, Y.-Z., Heger, A., & Haxton, W. C. 2016, NatCo, 7, 13639
Bao, Z. Y., Beer, H., Käppeler, F., et al. 2000, ADNDT, 76, 70
Bauswein, A., Goriely, S., & Janka, H.-T. 2013, ApJ, 773, 78
Becker, S. A., & Iben, I., Jr. 1979, ApJ, 232, 831
Bisterzo, S., Travaglio, C., Gallino, R., Wiescher, M., & Käppeler, F. 2014, ApJ, 787, 10
Bojazi, M. J., & Meyer, B. S. 2017, LPSC, 48, 3010
Bojazi, M. J., & Meyer, B. S. 2018, LPSC, 49, 2890
Bondarenko, V., Berzins, J., Prokofjevs, P., et al. 2002, NuPhA, 709, 3
Boss, A. P. 2003, in ASP Conf. Ser. 287, Galactic Star Formation Across the Stellar Mass Spectrum, ed. J. M. De Buizer & N. S. van der Bliek (San Francisco, CA: ASP), 281
Boss, A. P. 2017, ApJ, 844, 113
Branch, D., & Wheeler, J. C. 2017, Supernova Explosions (Berlin: Springer)
Brennecka, G. A., Weyer, S., Wadhwa, M., et al. 2010, Sci, 327, 449
Burkhardt, C., Kleine, T., Bourdon, B., et al. 2008, GeCoA, 72, 6177
Busso, M. 2011, LNP, 812, 309
Busso, M. 2018, LNP, in press
Busso, M., Gallino, R., & Wasserburg, G. J. 1999, ARA&A, 37, 239
Busso, M., Gallino, R., & Wasserburg, G. J. 2003, PASA, 20, 356
Busso, M., Palmerini, S., Maiorca, E., et al. 2010, ApJL, 717, L47
Busso, M., Wasserburg, G. J., Nollett, K. M., & Calandra, A. 2007, ApJ, 671, 802
Cameron, A. G. W., Thielemann, F.-K., & Cowan, J. J. 1993, PhR, 227, 283
Cameron, A. G. W., & Truran, J. W. 1977, Icar, 30, 447
Charbonnel, C., & Lagarde, N. 2010, A&A, 522, A10
Charbonnel, C., & Zahn, J.-P. 2007, A&A, 476, L29
Chaussidon, M., Robert, F., & McKeegan, K. D. 2006, GeCoA, 70, 224
Chieffi, A., & Limongi, M. 2013, ApJ, 764, 21
Chieffi, A., & Limongi, M. 2015, in IAU Symp. 307, New Windows on Massive Stars, ed. G. Meynet et al. (Cambridge: Cambridge Univ. Press), 1
Clayton, R. N. 2003, TrGeo, 1, 711
Côté, B., Belczynski, K., Fryer, C. L., et al. 2017, ApJ, 836, 230
Cristallo, S., Abia, C., Straniero, O., & Piersanti, L. 2015a, ApJ, 801, 53
Cristallo, S., Di Leva, A., Imbriani, G., et al. 2014, A&A, 570, A46
Cristallo, S., Karinkuzhi, D., Goswami, A., Piersanti, L., & Gobrecht, D. 2016, ApJ, 833, 181
Cristallo, S., Piersanti, L., Straniero, O., et al. 2011, ApJS, 197, 17
Cristallo, S., Straniero, O., Gallino, R., et al. 2009, ApJ, 696, 797
Cristallo, S., Straniero, O., Piersanti, L., & Gobrecht, D. 2015b, ApJS, 219, 40
Dauphas, N., John, S. G., & Rouxel, O. 2017, RvMG, 82, 415
Dauphas, N., & Schauble, E. A. 2016, AREPS, 44, 709

Davies, M. B., Adams, F. C., Armitage, P., et al. 2014, in Protostars and Planets VI, ed. H. Beuther et al. (Tucson, AZ: Univ. Arizona Press), 787
Davis, A. M., & McKeegan, K. D. 2014, TrGeo, 1, 361
Denissenkov, P. A., Herwig, F., Truran, J. W., & Paxton, B. 2013, ApJ, 772, 37
Denissenkov, P. A., & Merryfield, W. J. 2011, ApJL, 727, L8
Denissenkov, P. A., & Tout, C. A. 2003, MNRAS, 340, 722
Diehl, R., Halloin, H., Kretschmer, K., et al. 2006, Natur, 439, 45
Dillmann, I. 2014, in XIII Nuclei in the Cosmos (NIC XIII), ed. Z. Elekes & Z. Fülöp (Trieste: PoS), 57
Dillmann, I., Kratz, K.-L., Wöhr, A., et al. 2003, PhRvL, 91, 162503
Doherty, C. L., Gil-Pons, P., Siess, L., & Lattanzio, J. C. 2017, PASA, 34, e056
Duprat, J., & Tatischeff, V. 2007, ApJL, 671, L69
Dwarkadas, V. V., Dauphas, N., Meyer, B., Boyajian, P., & Bojazi, M. 2017, ApJ, 851, 147
Dwarkadas, V. V., Dauphas, N., Meyer, B., Boyajian, P., & Bojazi, M. 2018, LPSC, 49, 1304
Eggleton, P. P., Dearborn, D. S. P., & Lattanzio, J. C. 2006, Sci, 314, 1580
Eggleton, P. P., Dearborn, D. S. P., & Lattanzio, J. C. 2008, ApJ, 677, 581
Eichler, D., Livio, M., Piran, T., & Schramm, D. N. 1989, Natur, 340, 126
Farouqi, K., Kratz, K.-L., Cowan, J. J., et al. 2008a, in AIP Conf. Ser. 990, First Stars III, ed. B. W. O'She & A. Heger (Melville, NY: AIP), 309
Farouqi, K., Kratz, K.-L., Mashonkina, L. I., Pfeiffer, B., & Thielemann, F.-K. 2008b, in AIP Conf. Ser. 1001, Evolution and Nucleosynthesis in AGB Stars, ed. R. Guanadalini, S. Palmerini, & M. Busso (Melville, NY: AIP), 245
Farouqi, K., Kratz, K.-L., & Pfeiffer, B. 2009, PASA, 26, 194
Farouqi, K., Kratz, K.-L., Pfeiffer, B., et al. 2010, ApJ, 712, 1359
Frebel, A., & Beers, T. C. 2018, PhT, 71, 30
Freiburghaus, C., Rosswog, S., & Thielemann, F.-K. 1999, ApJL, 525, L121
Fröhlich, C., Hix, W. R., Martínez-Pinedo, G., et al. 2006, NewAR, 50, 496
Gilroy, K. K. 1989, ApJ, 347, 835
Goriely, S., & Janka, H.-T. 2016, MNRAS, 459, 4174
Goriely, S., Sida, J.-L., Lemaître, J.-F., et al. 2013, PhRvL, 111, 242502
Goswami, J. N., & Vanhala, H. A. T. 2000, in Protostars and Planets IV, ed. V. Mannings, A. P. Boss, & S. S. Russell (Tucson, AZ: Univ. Arizona Press), 963
Gounelle, M., & Meynet, G. 2012, A&A, 545, A4
Gounelle, M., Shu, F. H., Shang, H., et al. 2006, ApJ, 640, 1163
Hansen, C. J., Primas, F., Hartman, H., et al. 2012, A&A, 545, A31
Hansen, T. T., Holmbeck, E. M., Beers, T. C., et al. 2018, ApJ, 858, 92
Hidaka, H., & Yoneda, S. 2013, NatSR, 3, 1330
Higdon, J. C., Lingenfelter, R. E., & Rothschild, R. E. 2004, ApJL, 611, L29
Hill, V., Christlieb, N., Beers, T. C., et al. 2017, A&A, 607, A91
Honda, S., Aoki, W., Ishimaru, Y., Wanajo, S., & Ryan, S. G. 2006, ApJ, 643, 1180
Huss, G. R., Goswami, J. N., Meyer, B. S., Sahijpal, S., & Wasserburg, G. J. 2007, LP, 1374, 71
Huss, G. R., Meyer, B. S., Srinivasan, G., Goswami, J. N., & Sahijpal, S. 2009, GeCoA, 73, 4922
Ji, A. P., Frebel, A., Ezzeddine, R., & Casey, A. R. 2016a, ApJL, 832, L3
Ji, A. P., Frebel, A., Simon, J. D., & Chiti, A. 2016b, ApJ, 830, 93
Kajino, T., & Mathews, G. J. 2017, RPPh, 80, 084901
Käppeler, F., Gallino, R., Bisterzo, S., & Aoki, W. 2011, RvMP, 83, 157
Kastner, J. H., & Myers, P. C. 1994, ApJ, 421, 605
Kratz, K.-L., Bitouzet, J.-P., Thielemann, F.-K., Moeller, P., & Pfeiffer, B. 1993, ApJ, 403, 216
Kratz, K. L., Farouqi, K., Hallmann, O., Pfeiffer, B., & Ott, U. 2014a, in AIP Conf. Ser. 1595, Seventh European Summer School on Experimental Nuclear Astrophysics, ed. C. Spitaleri, L. Lamia, & R. G. Pizzone (Melville, NY: AIP), 62
Kratz, K.-L., Farouqi, K., Mashonkina, L. I., & Pfeiffer, B. 2008, NewAR, 52, 390
Kratz, K.-L., Farouqi, K., & Möller, P. 2014b, ApJ, 792, 6
Kratz, K.-L., Pfeiffer, B., Cowan, J. J., & Sneden, C. 2004, NewAR, 48, 105
Lattimer, J. M., Schramm, D. N., & Grossman, L. 1977, Natur, 269, 116
Lee, T., Papanastassiou, D. A., & Wasserburg, G. J. 1976, GeoRL, 3, 109
Li, H., McCray, R., & Sunyaev, R. A. 1993, ApJ, 419, 824
Liu, M.-C., Chaussidon, M., Srinivasan, G., & McKeegan, K. D. 2012, ApJ, 761, 137
Liu, N., Savina, M. R., Davis, A. M., et al. 2014, ApJ, 786, 66
Liu, N., Savina, M. R., Gallino, R., et al. 2015, ApJ, 803, 12
Lodders, K. 2003, ApJ, 591, 1220
Lodders, K., & Palme, H. 2009, M&PSA, 72, 5154
Loll, A. M., Desch, S. J., Scowen, P. A., & Foy, J. P. 2013, ApJ, 765, 152
Lugaro, M., Doherty, C. L., Karakas, A. I., et al. 2012, M&PS, 47, 1998
Lugaro, M., Heger, A., Osrin, D., et al. 2014, Sci, 345, 650
Macias, P., & Ramirez-Ruiz, E. 2016, arXiv:1609.04826
Maeda, K., Kawabata, K., Mazzali, P. A., et al. 2008, Sci, 319, 1220
Martínez-Pinedo, G., Fischer, T., Langanke, K., et al. 2017, in Handbook of Supernovae, ed. A. W. Alsabti & P. Murdin (Berlin: Springer), 1805
Martínez-Pinedo, G., Fischer, T., Lohs, A., & Huther, L. 2012, PhRvL, 109, 251104
Mathews, G. J., Snedden, A., Phillips, L. A., et al. 2014, MPLA, 29, 1430012
McKeegan, K. D., Kallio, A. P. A., Heber, V. S., et al. 2011, Sci, 332, 1528
Meyer, B. S. 1989, ApJ, 343, 254
Meyer, B. S., & Clayton, D. D. 2000, SSRv, 92, 133
Möller, P. 2012, PhRvL, 108, 052501
Mostefaoui, S., Lugmair, G. W., & Hoppe, P. 2005, ApJ, 625, 271
Nichols, R. H., Jr., Podosek, F. A., Meyer, B. S., & Jennings, C. L. 1999, LPI, 30, 1790
Nishimura, N., Sawai, H., Takiwaki, T., Yamada, S., & Thielemann, F.-K. 2017, ApJL, 836, L21
Nollett, K. M., Busso, M., & Wasserburg, G. J. 2003, ApJ, 582, 1036
Nordhaus, J., Busso, M., Wasserburg, G. J., Blackman, E. G., & Palmerini, S. 2008, ApJL, 684, L29
Nucci, M. C., & Busso, M. 2014, ApJ, 787, 141
Ott, U., & Kratz, K.-L. 2008, NewAR, 52, 396
Palmerini, S., Cristallo, S., Busso, M., et al. 2011a, ApJ, 741, 26
Palmerini, S., La Cognata, M., Cristallo, S., & Busso, M. 2011b, ApJ, 729, 3
Palmerini, S., Trippella, O., & Busso, M. 2017, MNRAS, 467, 1193
Palmerini, S., Trippella, O., Busso, M., et al. 2018, GeCoA, 221, 21
Pan, L., Desch, S. J., Scannapieco, E., & Timmes, F. X. 2012, ApJ, 756, 102
Pastorello, A., Pumo, M. L., Navasardyan, H., et al. 2012, A&A, 537, A141
Pellin, M. J., Savina, M. R., Calaway, W. F., et al. 2006, LPI, 37, 2041
Pfeiffer, B., Ott, U., & Kratz, K.-L. 2001, NuPhA, 688, 575
Pian, E., D'Avanzo, P., Benetti, S., et al. 2017, Natur, 551, 67
Pignatari, M., Gallino, R., Heil, M., et al. 2010, ApJ, 710, 1557
Podosek, F. A., & Nichols, R. H. 1997, in AIP Conf. Ser. 402, Astrophysical Implications of the Laboratory Study of Presolar Materials, ed. T. J. Bernatowicz & E. Zinner (Melville, NY: AIP), 617
Poitrasson, F. 2017, RvMG, 82, 289
Qian, Y.-Z., & Wasserburg, G. J. 2000, PhR, 333, 77
Raiteri, C. M., Gallino, R., Busso, M., Neuberger, D., & Kaeppeler, F. 1993, ApJ, 419, 207
Reynolds, J. H. 1960, PhRvL, 4, 351
Roberts, L. F., Reddy, S., & Shen, G. 2012, PhRvC, 86, 065803
Roederer, I. U., Cowan, J. J., Karakas, A. I., et al. 2010, ApJ, 724, 975
Roederer, I. U., Kratz, K.-L., Frebel, A., et al. 2009, ApJ, 698, 1963
Roederer, I. U., Mateo, M., Bailey, J. I., III, et al. 2016, AJ, 151, 82
Rubin, M., Altwegg, K., Balsiger, H., et al. 2017, A&A, 601, A123
Sahijpal, S., Goswami, J. N., Davis, A. M., Grossman, L., & Lewis, R. S. 1998, Natur, 391, 559
Sakamoto, N., Seto, Y., Itoh, S., et al. 2007, Sci, 317, 231
Schönbächler, M., Carlson, R. W., Horan, M. F., Mock, T. D., & Hauri, E. H. 2008, GeCoA, 72, 5330
Siegel, D. M., & Metzger, B. D. 2017, PhRvL, 119, 231102
Sneden, C., Cowan, J. J., & Gallino, R. 2008, ARA&A, 46, 241
Sneden, C., McWilliam, A., Preston, G. W., et al. 1996, ApJ, 467, 819
Solomon, P. M., Sanders, D. B., & Scoville, N. Z. 1979, in IAU Symp. 84, The Large-Scale Characteristics of the Galaxy, ed. W. B. Burton (Dordrecht: Reidel), 35
Sossi, P. A., Moynier, F., Chaussidon, M., et al. 2017, NatAs, 1, 0055
Spite, F., Spite, M., Barbuy, B., et al. 2018, A&A, 611, A30
Spitzer, L. 1962, Physics of Fully Ionized Gases (2nd ed.; New York: Interscience)
Srinivasan, G., Sahijpal, S., Ulyanov, A. A., & Goswami, J. N. 1996, GeCoA, 60, 1823
Srinivasan, G., Ulyanov, A. A., & Goswami, J. N. 1994, ApJL, 431, L67
Straniero, O., Gallino, R., & Cristallo, S. 2006, NuPhA, 777, 311
Takigawa, A., Miki, J., Tachibana, S., et al. 2008, ApJ, 688, 1382
Tang, H., & Dauphas, N. 2012, E&PSL, 359, 248
Tanvir, N. R., Levan, A. J., González-Fernández, C., et al. 2017, ApJL, 848, L27
Tatischeff, V., Duprat, J., & de Séréville, N. 2014, ApJ, 796, 124
Telus, M., Huss, G. R., Ogliore, R. C., et al. 2016, GeCoA, 178, 87
Teng, F.-Z. 2017, RvMG, 82, 219
Thielemann, F.-K., Eichler, M., Panov, I. V., & Wehmeyer, B. 2017, ARNPS, 67, 253
Thielemann, F.-K., Isern, J., Perego, A., & von Ballmoos, P. 2018, SSRv, 214, 62

Thompson, T. A., & ud-Doula, A. 2018, MNRAS, 476, 5502
Trappitsch, R., Boehnke, P., Stephan, T., et al. 2018, ApJL, 857, L15
Trigo-Rodríguez, J. M., García-Hernández, D. A., Lugaro, M., et al. 2009, M&PS, 44, 627
Trippella, O., Busso, M., Maiorca, E., Käppeler, F., & Palmerini, S. 2014, ApJ, 787, 41
Trippella, O., Busso, M., Palmerini, S., Maiorca, E., & Nucci, M. C. 2016, ApJ, 818, 125
Troja, E., Piro, L., van Eerten, H., et al. 2017, Natur, 551, 71
Tsujimoto, T., Matsuno, T., Aoki, W., Ishigaki, M. N., & Shigeyama, T. 2017, ApJL, 850, L12
Tsujimoto, T., & Shigeyama, T. 2001, ApJL, 561, L97
Umeda, H., & Nomoto, K. 2002, ApJ, 565, 385
Utrobin, V. P., & Chugai, N. N. 2005, A&A, 441, 271
Vangioni, E., Goriely, S., Daigne, F., François, P., & Belczynski, K. 2016, MNRAS, 455, 17
Vanhala, H. A. T., & Boss, A. P. 2002, ApJ, 575, 1144
Villeneuve, J., Chaussidon, M., & Libourel, G. 2009, Sci, 325, 985
Wadhwa, M., Amelin, Y., Davis, A. M., et al. 2007, Protostars and Planets V, 835
Wanajo, S., & Janka, H.-T. 2012, ApJ, 746, 180
Wanajo, S., Sekiguchi, Y., Nishimura, N., et al. 2014, ApJL, 789, L39
Wasserburg, G. J., Boothroyd, A. I., & Sackmann, I.-J. 1995, ApJL, 447, L37
Wasserburg, G. J., Busso, M., & Gallino, R. 1996, ApJL, 466, L109
Wasserburg, G. J., Busso, M., Gallino, R., & Nollett, K. M. 2006, NuPhA, 777, 5
Wasserburg, G. J., Busso, M., Gallino, R., & Raiteri, C. M. 1994, ApJ, 424, 412
Wasserburg, G. J., Gallino, R., & Busso, M. 1998, ApJL, 500, L189
Wasserburg, G. J., Gallino, R., Busso, M., Goswami, J. N., & Raiteri, C. M. 1995, ApJL, 440, L101
Wasserburg, G. J., Karakas, A. I., & Lugaro, M. 2017, ApJ, 836, 126
Wasserburg, G. J., Trippella, O., & Busso, M. 2015, ApJ, 805, 7
Woosley, S. E., Wilson, J. R., Mathews, G. J., Hoffman, R. D., & Meyer, B. S. 1994, ApJ, 433, 229